

# UNCLASSIFIED

AD NUMBER
AD865977
NEW LIMITATION CHANGE
TO Approved for public release, distribution unlimited
FROM Distribution authorized to U.S. Gov't. agencies and their contractors; Administrative/Operational Use; OCT 1969. Other requests shall be referred to Air Force Propulsion Lab., Edwards AFB, CA.
AUTHORITY
AFRPL ltr 29 Sep 1971

THIS PAGE IS UNCLASSIFIED

AD 865977

AFRPL-TR-69-203

# TEST FIRING OF A SUPERSONIC SPLIT-LINE NOZZLE

R. K. STROME, LT, USAF

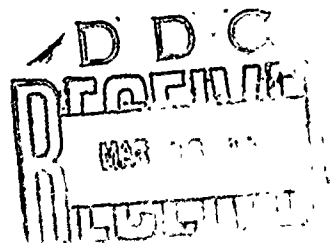
TECHNICAL REPORT AFRPL-TR-69-203

OCTOBER 1969

THIS DOCUMENT IS SUBJECT TO SPECIAL EXPORT CONTROLS AND EACH  
TRANSMITTAL TO FOREIGN GOVERNMENTS OR FOREIGN NATIONALS MAY  
BE MADE ONLY WITH APPROVAL OF AFRPL (RPOR-STINFO), EDWARDS,  
CALIFORNIA 93523.

AIR FORCE ROCKET PROPULSION LABORATORY  
AIR FORCE SYSTEMS COMMAND  
UNITED STATES AIR FORCE  
EDWARDS, CALIFORNIA

Reproduced by the  
CLEARINGHOUSE  
for Federal Scientific & Technical  
Information Springfield Va. 22151



AFRPL-TR-69-203

TEST FIRING OF A SUPERSONIC SPLIT-LINE NOZZLE

R.K. Strome, Lt, USAF

This document is subject to special export controls and each transmittal to foreign governments or foreign nationals may be made only with approval of AFRPL (RPOR-STINFO), Edwards, California 93523.

## NOTICES

When U. S. Government drawings, specifications, or other data are used for any purpose other than a definitely related Government procurement operation, the fact that the Government may have formulated, furnished, or in any way supplied the said drawings, specifications, or other data, is not to be regarded by implication or otherwise, or in any manner licensing the holder or any other person or corporation, or conveying any rights or permission to manufacture, use, or sell any patented invention that may in any way be related thereto.

ACCESSION IN	
OFSTI	WHITE SECTION <input type="checkbox"/>
DOC	BWF SECTION <input checked="" type="checkbox"/>
UNANNOUNCED, <input type="checkbox"/>	
JUSTIFICATION .....	
BY .....	
DISTRIBUTION/AVAILABILITY CODES	
DIST.	AVAIL. and/or SPECIAL
2	

## FOREWORD

This report was prepared by the Motor Component Development Branch, Solid Rocket Division, Air Force Rocket Propulsion Laboratory (AFRPL). The subject test was conducted at AFRPL under Project 305903 AMG, Solid Rocket Design and Evaluation (SRHDE), on 29 January 1969. Lt R.K. Strome was Project Engineer for this particular test. The nozzle being evaluated was designed by ARDE Portland, Inc., under subcontract to Rocketdyne, McGregor, Texas. Mr. Durwood Thrasher was the project technical advisor responsible for the checkout of the nozzle. Rocketdyne has performed a posttest analysis of the nozzle.

CHARLES R. COOKE  
Chief, Solid Rocket Division  
Air Force Rocket Propulsion Laboratory

## TABLE OF CONTENTS

<u>Section</u>	<u>Page</u>
I INTRODUCTION . . . . .	1
II CONCEPT . . . . .	2
III TVC SYSTEM DESIGN DESCRIPTION AND NOZZLE DESCRIPTION . . . . .	9
A. Introduction . . . . .	9
B. Nozzle Description . . . . .	9
C. Actuation System . . . . .	16
IV AFRPL PROGRAMMER SYSTEM . . . . .	20
V TEST . . . . .	26
A. Equipment . . . . .	26
1. Thrust Stand . . . . .	26
2. Motor . . . . .	28
3. Propellant and Igniters . . . . .	28
B. Firing . . . . .	30
C. Nozzle Posttest Condition . . . . .	30
VI TEST RESULTS . . . . .	37
A. Data Reduction . . . . .	37
B. Data Interpretation . . . . .	41
C. Data Evaluation . . . . .	51
VII CONCLUSIONS AND RECOMMENDATIONS . . . . .	53
REFERENCES . . . . .	67

# TABLE OF CONTENTS (Cont)

<u>Section</u>	<u>Page</u>
APPENDIX - Calculations and System Checkout . . .	69
A. Calculation of Friction Torque . . .	69
B. Determination of Torque Equation . . .	71
C. Nozzle Ballistic Performance . . .	72
D. TVC System Checkout . . .	73
E. PLOTS . . .	76
DISTRIBUTION . . .	87
FORM 1473 . . .	93

## FIGURES

<u>Figure</u>		<u>Page</u>
1	Comparison Between Supersonic and Subsonic Split-line Nozzles . . . . .	3
2	Supersonic Flow In Supersonic Split-line (SSSL) Nozzle	4
3	Forces on Nozzle Movable Section . . . . .	5
4	Supersonic Split-line Moment Arm . . . . .	7
5	TVC Electrical Schematic . . . . .	10
6	TVC Hydraulic Schematic . . . . .	11
7	External View of Nozzle . . . . .	13
8	Supersonic Split-line Nozzle Material Description .	14
9	Supersonic Split-line Nozzle Dimensions . .	15
10	Omniaxis Vectoring with a Gimbal Support . .	17
11	Nozzle in Deflected Position . . . . .	18
12	Supersonic Split-line Programmer System . .	22
13	Programmer System State, T = 0 sec. . . . .	23
14	Programmer System State, T = 1 sec. . . . .	24
15	Programmer System State, T = 2 sec. . . . .	25
16	Thrust Stand and Assembled Motor . . . . .	27
17	Pyrogen Igniter on Motor . . . . .	29
18	Top of Nozzle, Prefire . . . . .	31
19	Postfire Nozzle, Side View . . . . .	33
20	Postfire Nozzle, Top View . . . . .	34
21	Postfire Nozzle, Top View . . . . .	35
22	Postfire Nozzle, Bottom View . . . . .	36



# FIGURES (Cont)

<u>Figure</u>		<u>Page</u>
23	Axial Thrust and Thrust Vector versus Time . . . . .	54
24	Chamber Pressure versus Time . . . . .	55
25	Y side force versus Time . . . . .	56
26	X side force versus Time . . . . .	57
27	Actual Nozzle Angle and Programmed Nozzle Angle versus Time . . . . .	58
28	Side Force versus Time . . . . .	59
29	Actual Pitch Angle versus Time . . . . .	60
30	Torque (Pitch) versus Time . . . . .	61
31	Pitch Angle versus Torque . . . . .	62
32	Actual Yaw Angle versus Time . . . . .	63
33	Torque (Yaw) versus Time . . . . .	64
34	Yaw Angle versus Torque . . . . .	65
35	Actual Nozzle Angle versus Side Force . . . . .	66
36	Nozzle Actuators . . . . .	71
37	Plotted Chamber Pressure . . . . .	77
38	Plotted Thrust . . . . .	78
39	Plotted X Side Force . . . . .	79
40	Plotted Y Side Force . . . . .	80
41	Plotted Yaw Torque . . . . .	81
42	Plotted Pitch Torque . . . . .	82
43	Yaw Output Volts . . . . .	83
44	Pitch Output Volts . . . . .	84

## FIGURES (Cont)

<u>Figure</u>	<u>Page</u>
45      Plotted Thrust Vector . . . . .	85
46      Plotted Side Force . . . . .	86

## TABLES

<u>Table</u>	<u>Page</u>
I      Amplification Factor . . . . .	44
II      Friction Work . . . . .	49
III      Friction Torque . . . . .	49
IV      Revised Friction Torque . . . . .	50

# LIST OF SYMBOLS

$\theta, \dot{\theta}, \ddot{\theta}$	Nozzle angle	degrees
$F_S$	Side force	pounds
$F_A$	Axial thrust	pounds
$T$	Torque	inch-pounds
$J$	Moment of inertia of nozzle	$\text{in}^4$
$C_F$	Discharge coefficient of nozzle	dimensionless
$v_i$	Command voltage	volts
$E$	Error difference signal	volts
$Q$	Hydraulic oil flow	pounds per second
$\theta_1$	Nozzle angle before feedback	degrees
$v_F$	Feedback voltage	volts
$F_{ZCOR}$	Corrected thrust	pounds
$Z$	Load indicated by Z load cell	pounds
$W_p$	Burn rate	pounds per second
$t$	Time	seconds
$T_{yaw}$	Torque required by yaw actuator	inch-pounds
$T_{pitch}$	Torque required by pitch actuator	inch-pounds
$YawP$	Yaw pressure extend	psi
$YawR$	Yaw pressure retract	psi
$PP$	Pitch pressure extend	psi
$PR$	Pitch pressure retract	psi
$\phi$	Angle of thrust vector	degrees
$F_x$	X direction side force	pounds

# LIST OF SYMBOLS (Cont)

$F_y$	Y direction side force	pounds
$F_z$	Z direction force	pounds
P	Pitch angle	degrees
Y	Yaw angle	degrees
AMF	Amplification factor	dimensionless
$\mu$	Coefficient of friction	dimensionless
$T_w$	Total work	inch-pounds
$F_w$	Frictional work	inch-pounds

## SECTION I

### INTRODUCTION

Thrust vector control of solid propellant rockets by the use of gimbaled, swiveled, or rotating nozzles is well established. One nozzle type which has not been completely explored is the supersonic splitline gimbaled nozzle. This device is also called the "flexible skirt" nozzle and consists of a fixed entrance section and throat extension with the main portion of the exit cone being a separate movable unit. The flow turning occurs downstream of the throat in the supersonic region of flow. Movement of the exit cone is accomplished by a hydraulic actuator.

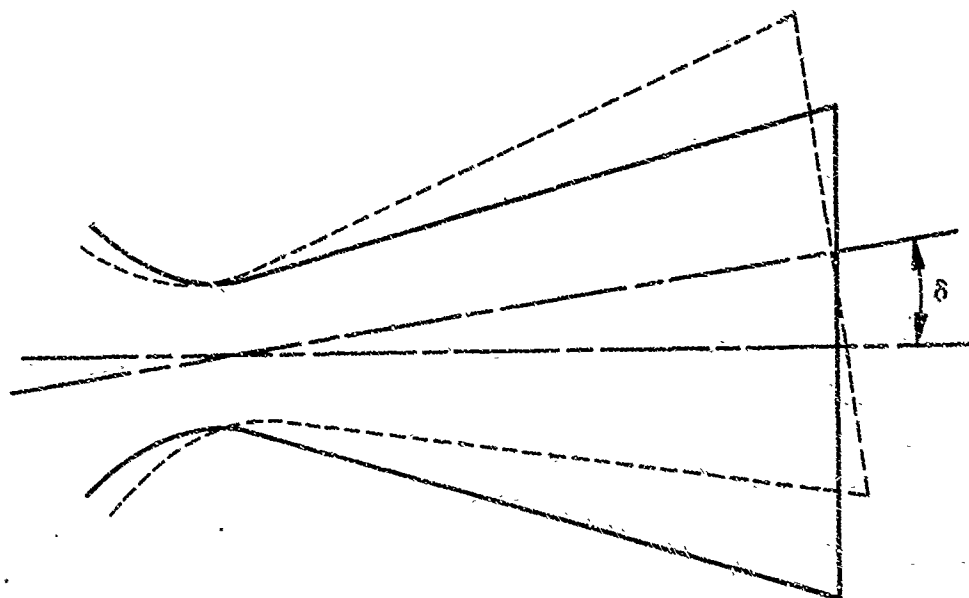
Solid propellant missile systems which favor the consideration of this steering method include: (a) systems requiring high deflections of thrust; and (b) systems with a limited lateral envelope for movement of the nozzle. Because of the characteristics of the supersonic splitline nozzle, thrust deflection is greater than nozzle deflection. Other advantages of this type nozzle, compared to a subsonic split-line gimbaled nozzle are: a split-line in a lower pressure region, a fixed entrance section, and greatly reduced axial loads on the gimbal ring. A primary uncertainty associated with the supersonic split-line nozzle is the actuation torque requirement for vectoring. This influences the sizing of the actuation system, and compatibility with the control system. In this nozzle, a primary contributor to the torque level is the turning of supersonic flow. This does not occur in other types of gimbaled nozzles. This report concerns itself with the experimental determination of the Force Amplification Factor and the torque levels required to actuate a particular supersonic split-line nozzle.

## SECTION II

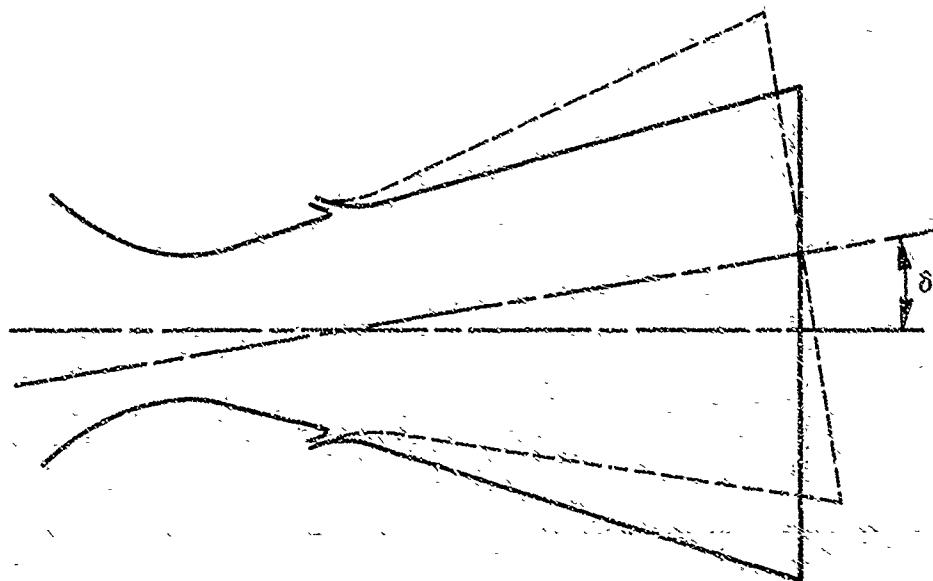
### CONCEPT

The supersonic split-line nozzle (Figure 1) is capable of producing thrust vector control in a solid propellant motor. This concept consists of a fixed entrance section and portion of the exit cone, with the majority of the exit cone being a separate movable unit sealed to the fixed portion of the nozzle on a spherical bearing surface. Movement of the exit cone about the seal point is accomplished by a hydraulic actuator. With a subsonic split-line nozzle, most of the flow turning occurs in the subsonic region upstream of the throat, and the degree of jet deflection is generally equal to the degree of nozzle rotation. With the supersonic split-line, however, shock-wave phenomena associated with supersonic flow can produce a jet deflection greater than the nozzle rotation.

In the design of a gimbaled nozzle, the objective is to obtain maximum thrust vectoring efficiency for conditions of minimum actuation torque. The pressure differential across the gap where the movable and fixed portion of the nozzle meet contributes to the development of nozzle side forces in the exit cone located downstream of the split-line, or gap. These side forces are caused by the strength of expansion and shock waves which originate at the gap and propagate downstream from the split-line as illustrated in Figure 2. The actuator must overcome these forces to deflect the nozzle through an angle  $\delta$  (Figure 1). Thus, the turning of supersonic flow with associated shock waves and pressure differentials downstream from the gap causes significant side forces to be developed. These side forces are directly proportional to the amount of torque required to deflect the nozzle. Other forces which contribute torque to the movable nozzle are illustrated in Figure 3 and described below.



Subsonic Split-line Nozzle



Supersonic Split-line Nozzle

Figure 1. Comparison Between Supersonic and Subsonic Split-line Nozzle.

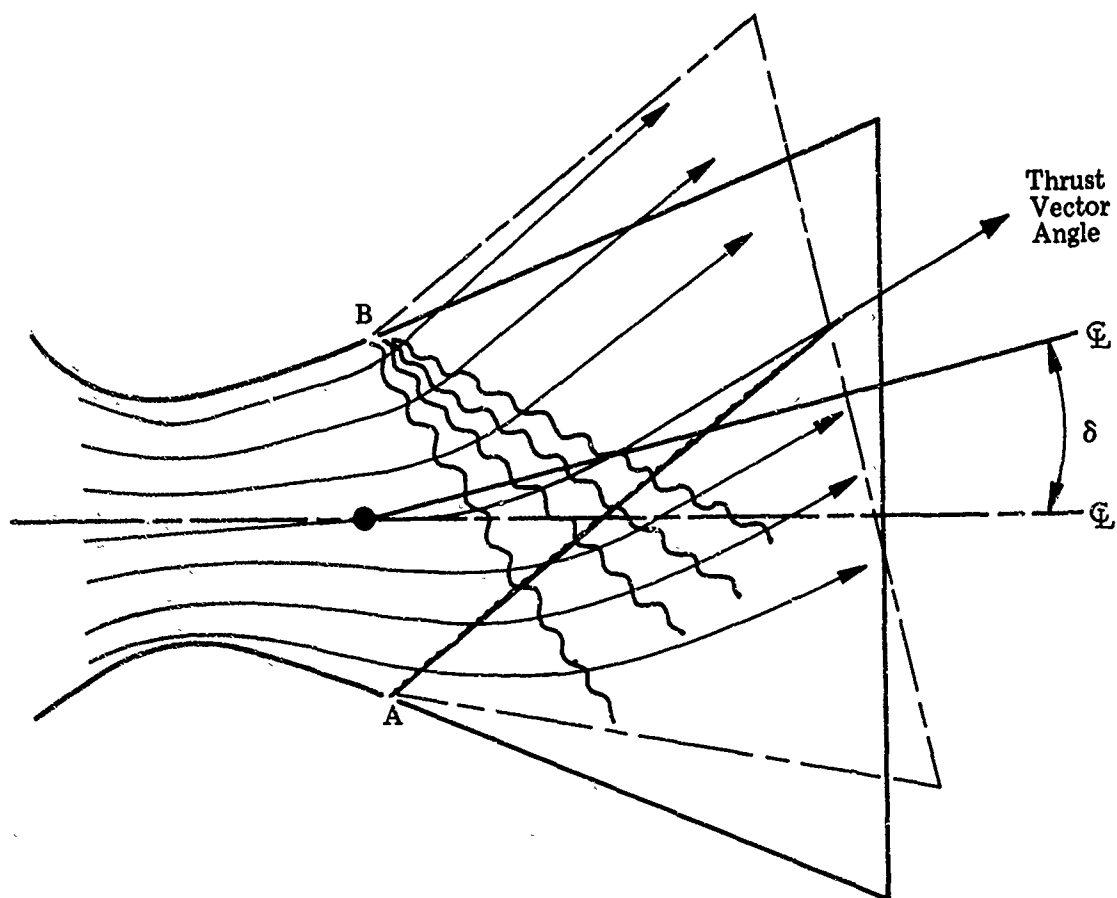






Figure 2. Supersonic Flow in Supersonic Split-line Nozzle.

According to supersonic flow theory, when supersonic flow is turned through an angle less than  $180^\circ$ , a shock wave is formed as at point A. When flow is turned greater than  $180^\circ$ , expansion or Mach waves are formed as at Point B.

Shock Wave   
 Expansion Wave   
 Flow Streamlines   
 Nozzle Pivot Point 

Due to the above propagations, the thrust vector angle can be greater than the nozzle angle  $\delta$ .



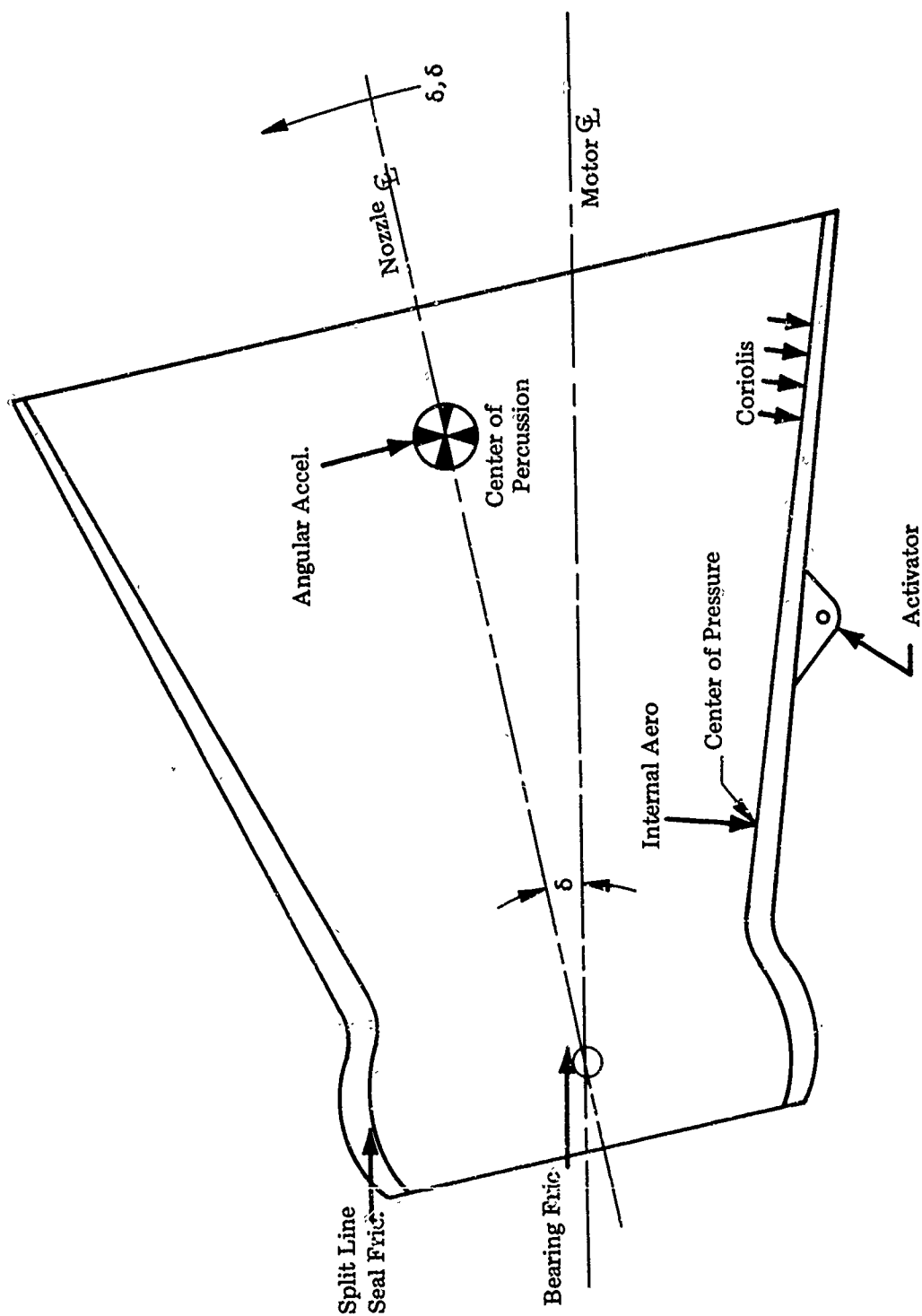


Figure 3. Forces on Nozzle Movable Section.

Friction. The friction torque results from the split-line seal and from the movable nozzle support bearings. Both of these factors are related to chamber pressure.

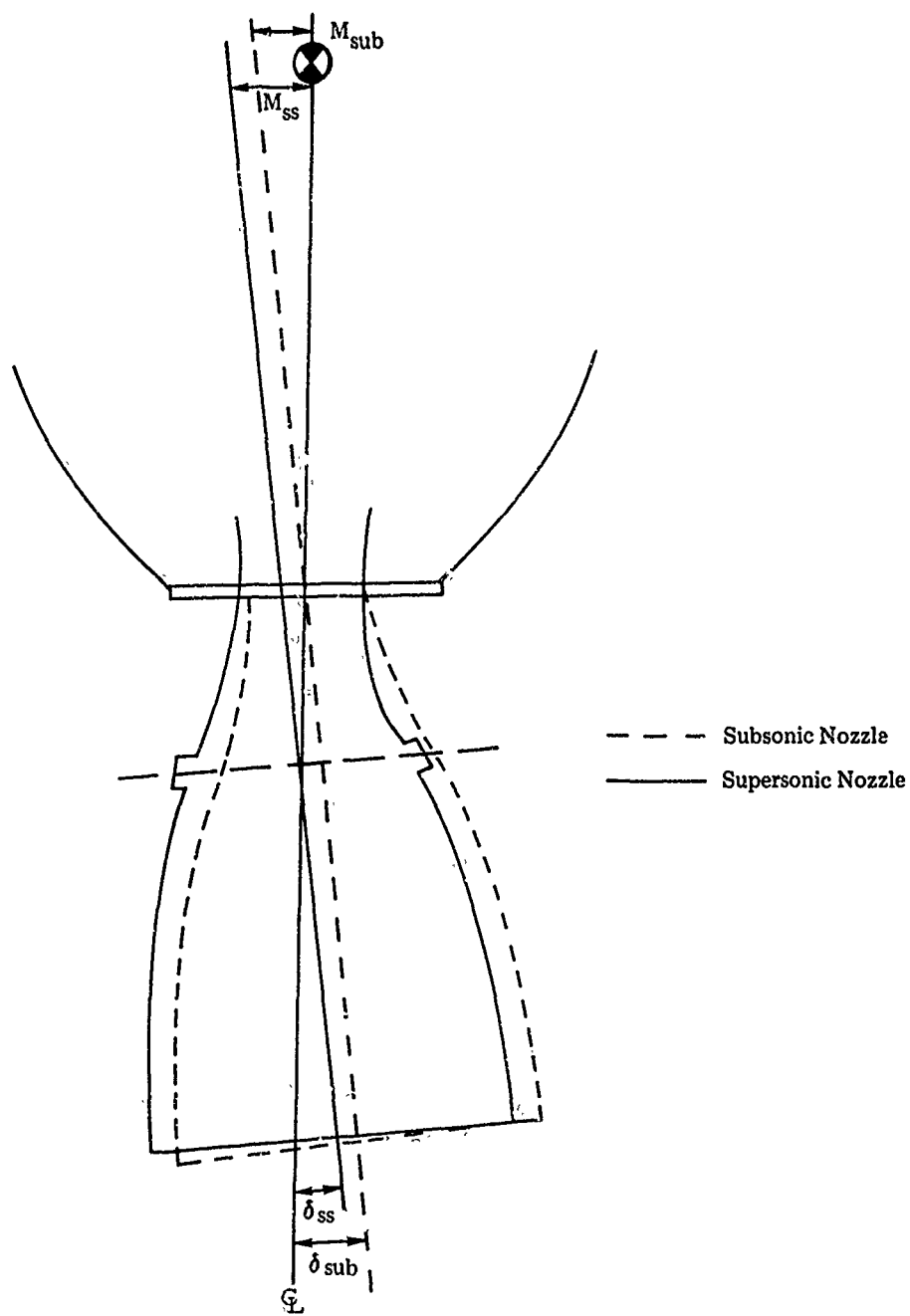
Internal Aerodynamics. The aerodynamic torque is the net moment on the movable portion of the nozzle due to the turning of the gases to some vector angle and is a function of nozzle geometry and chamber pressure.

Gas Coriolis. This torque arises from the mass translation within the rotating nozzle during movement from one vector angle to another which is represented by the flow of gas through the length of the nozzle. The Coriolis torque is a function of mass flow rate, nozzle length, and the instantaneous angular velocity of the nozzle.

Nozzle Angular Acceleration. Any net unbalance in torque will result in an angular acceleration or deceleration of the nozzle. The rate of acceleration or deceleration is proportional to the instantaneous net unbalanced torque, and inversely proportional to the polar mass moment of inertia of the movable portion of the nozzle:  $T = J\ddot{\theta}$

Because of the characteristics of the supersonic split-line nozzle, the moment arm about the vehicle center of gravity is greater, as can be seen in Figure 4, than that of the subsonic split-line nozzle. The SSSL nozzle is, therefore, capable of producing a larger turning torque on a vehicle in flight.

The effectiveness of a supersonic split-line is defined by the Force Amplification Factor, which is the ratio of the thrust vector angle to the actual nozzle position angle. This is also equal to  $F_s / (F_a \sin \delta)$ , where  $F_s$  is the side force,  $F_a$  the axial thrust, and  $\delta$  the nozzle rotation angle. The characteristics of supersonic flow deflection are significantly different from those of subsonic deflections because of the propagation of disturbances according to wave theory in supersonic flow (Figure 2).



$\delta_{ss}$  = Supersonic Split-line Nozzle deflection angle  
 $\delta_{sub}$  = Subsonic split-line nozzle deflection angle  
 $M_{ss}$  = Supersonic split-line moment arm  
 $M_{sub}$  = Subsonic split-line moment arm

Figure 4. Supersonic Split-line Moment Arm.

Thus, because of the propagations, the Force Amplification Factor for a supersonic split-line nozzle is theoretically greater than 1.0, i.e., the thrust vector angle is greater than the nozzle deflection angle.

## SECTION III

### TVC SYSTEM DESIGN DESCRIPTION AND NOZZLE DESCRIPTION

#### A. INTRODUCTION

The supersonic split-line nozzle was designed and built by Arde Portland, Inc., Paramus, New Jersey. This thrust vector control (TVC) rocket nozzle employs a fixed throat with an omniaxis gimbaled nozzle skirt. It utilizes a closed-loop hydraulic system, controlled by electro-hydraulic servo valves and electrical nozzle position feedback, to position the nozzle in accordance with an external command signal. The TVC system was designed to provide a maximum thrust vector angle of  $\pm 4$  degrees in both pitch and yaw planes.

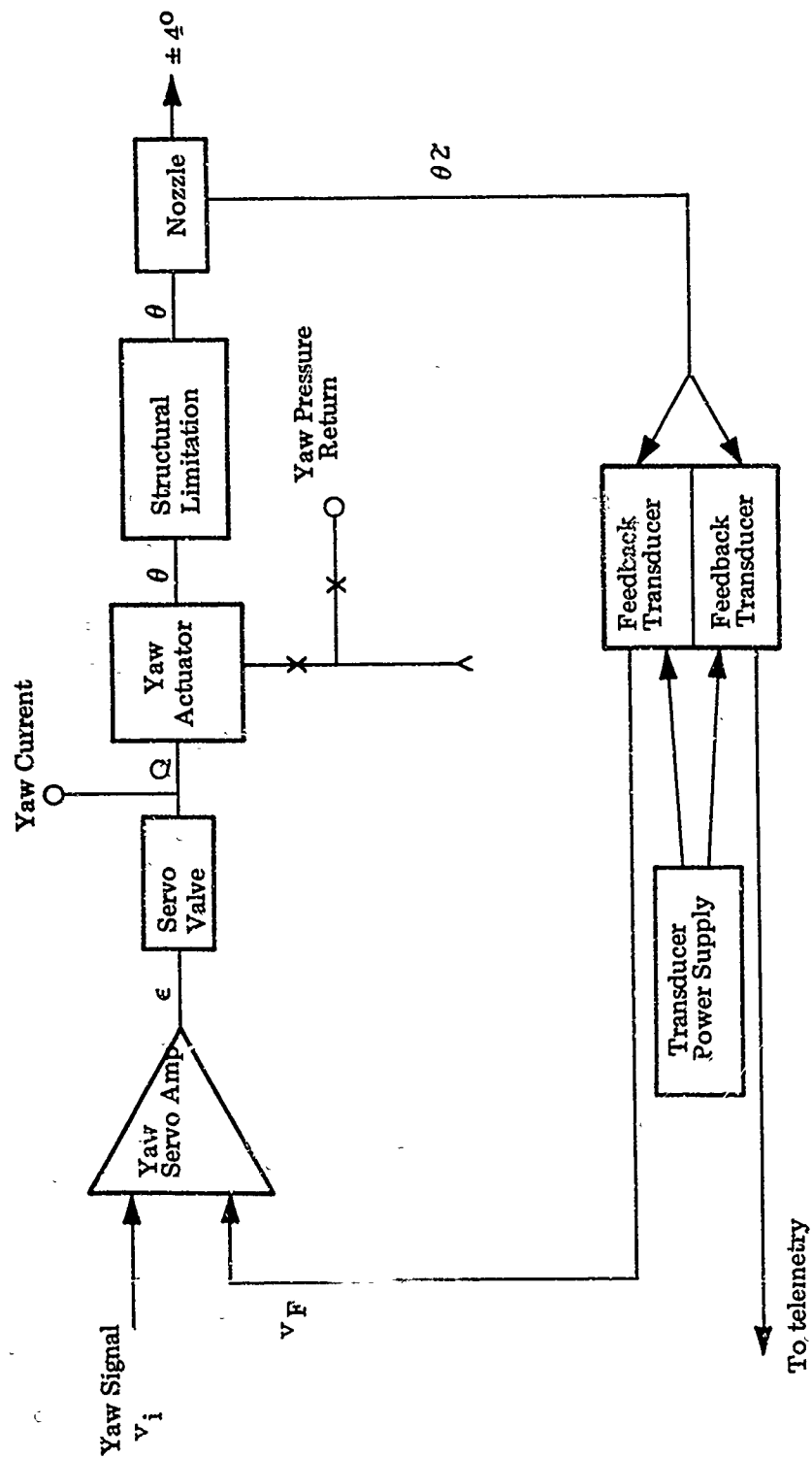
#### B. NOZZLE DESCRIPTION

The nozzle divergent geometry is a modified bell contour giving a theoretical minimum design nozzle efficiency of 96.4 percent in the nonactuated position. Design nozzle efficiency is calculated by the following expression:

$$\text{Nozzle efficiency (N}_c\text{) Percent} = \frac{C_F \text{ (calculated)}}{C_F \text{ (theoretical)}} \times 100$$

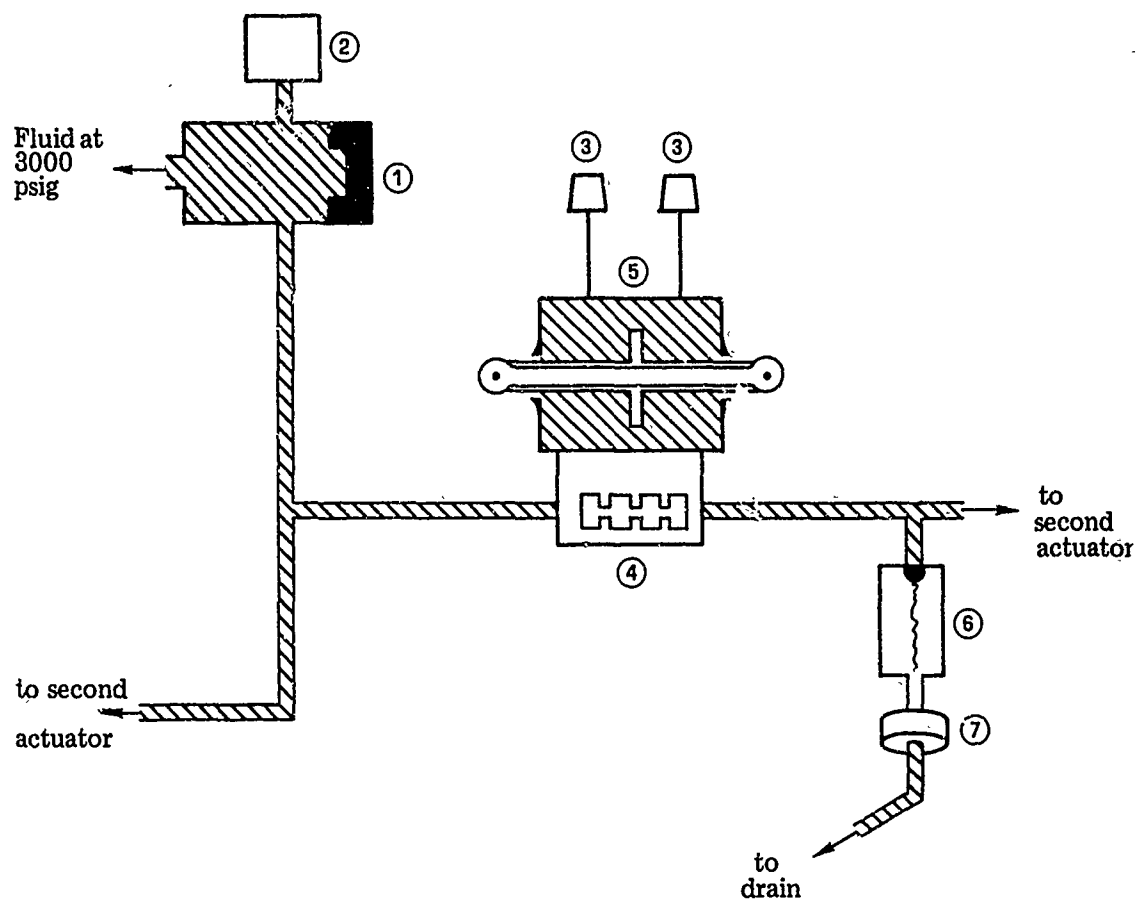
The terms used for the above equation are shown in Appendix, Section C.

The TVC system was designed for minimum weight consistent with performance requirements. This weight was about 90 pounds, including all mounting brackets and pressure lines, but not including attachments for monitoring pressure and other performance parameters. The TVC actuation system consisted of electrical (Figure 5) and hydraulic (Figure 6) systems. The hydraulic system was closed-loop, designed to utilize an existing hydraulic power unit. During the duty cycle, the hydraulic fluid was continuously filtered through a 10-micron element. There was



Pitch and Yaw Schematics are Identical

Figure 5. TVC Electrical Schematic



- 1 QUICK DISCONNECT
- 2 HYDRAULIC PRESSURE TRANSDUCER
- 3 PITCH & YAW EXTEND & RETURN PRESSURE TRANSDUCER
- 4 SERVOVALVE
- 5 ACTUATOR
- 6 OVERBOARD RELIEF VALVE
- 7 RUPTURE DISK

Figure 6. TVC Hydraulic Schematic

no system response degradation during static firing due to contamination. The hydraulic system was designed for a  $2000 \pm 200$  psi supply pressure, although a 3000 psi source was utilized for the static test.

The nozzle (Figure 7) consisted of three major components:

1. The inlet assembly (Figures 8 and 9)
2. The movable assembly (Figures 8 and 9)
3. The gimbal-ring assembly

The location of the split-line was placed in the supersonic region of gas flow optimized on the basis of seal protection, minimum aerodynamic losses and minimum weight. The inlet assembly was fixed on the aft closure of the motor and included the inlet gas passage, nozzle throat, sealing surface, and the support for the gimbal ring.

The movable assembly included the split-line seal, divergent section, and structural support system. The split-line between fixed and movable nozzle members was a ball and socket arrangement formed by spherical surfaces on the inlet and movable exit cone. The clearance space in the split-line was filled with a combination of materials consisting of silicone rubber, silicone grease, and zinc chromate, which limits gas circulation and provides lubrication. Gas sealing was provided by an O-ring made of buna-n rubber. The nozzle achieved omni-axial vectoring capability by the use of a gimbal ring.

#### 1. Inlet Assembly

Edge grain pyrolytic graphite washers formed the throat of the nozzle. The divergent sections upstream and downstream of the throat were made of high-density AHDG-HT graphite. Further downstream, graphite cloth (FM 5128) was used up to and including the nozzle split line. Behind the throat section, a sleeve of Grafoil No. 100 was used as a high-temperature insulating material. A neoprene washer was used between



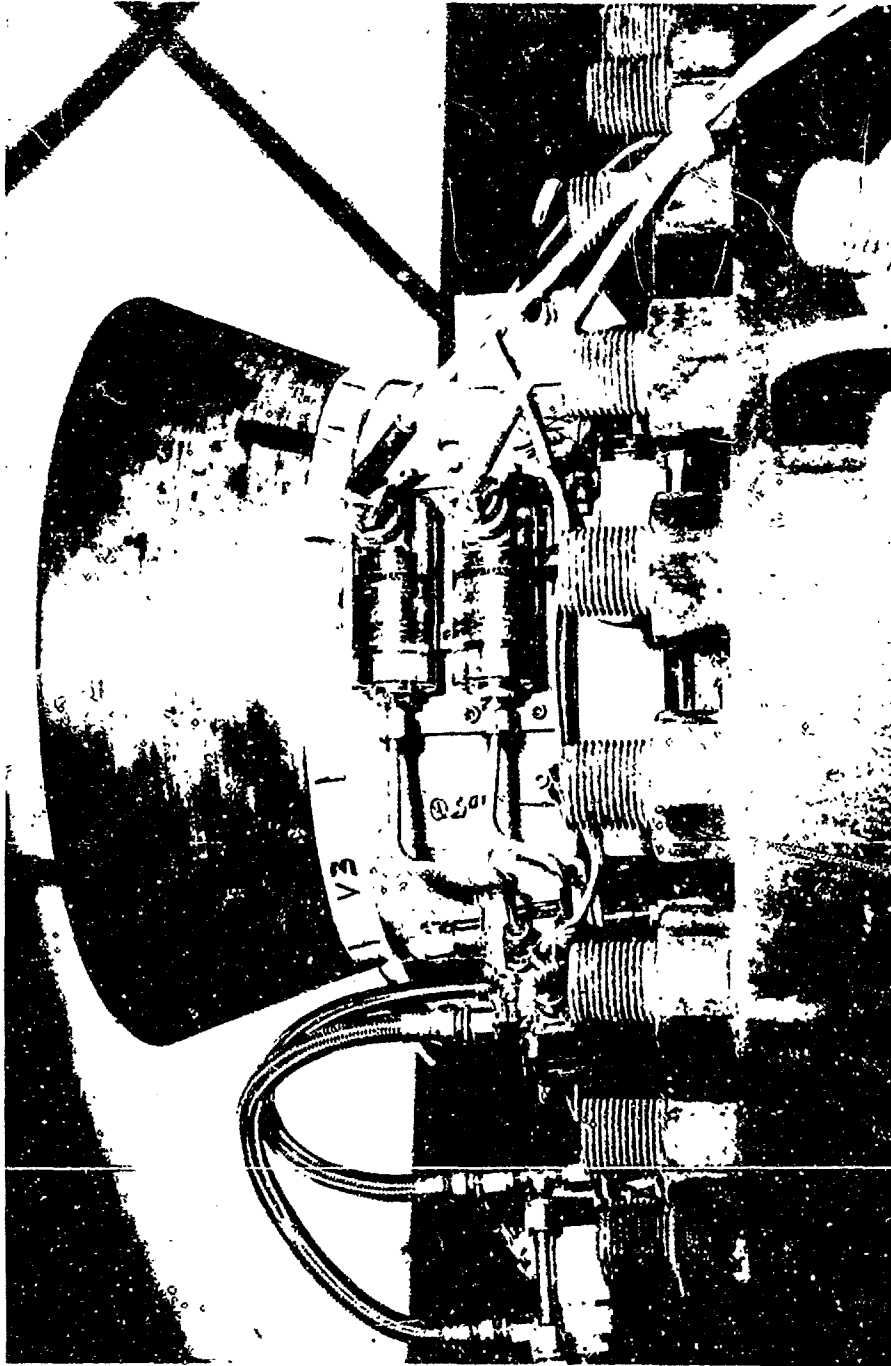


Figure 7. External View of Nozzle.

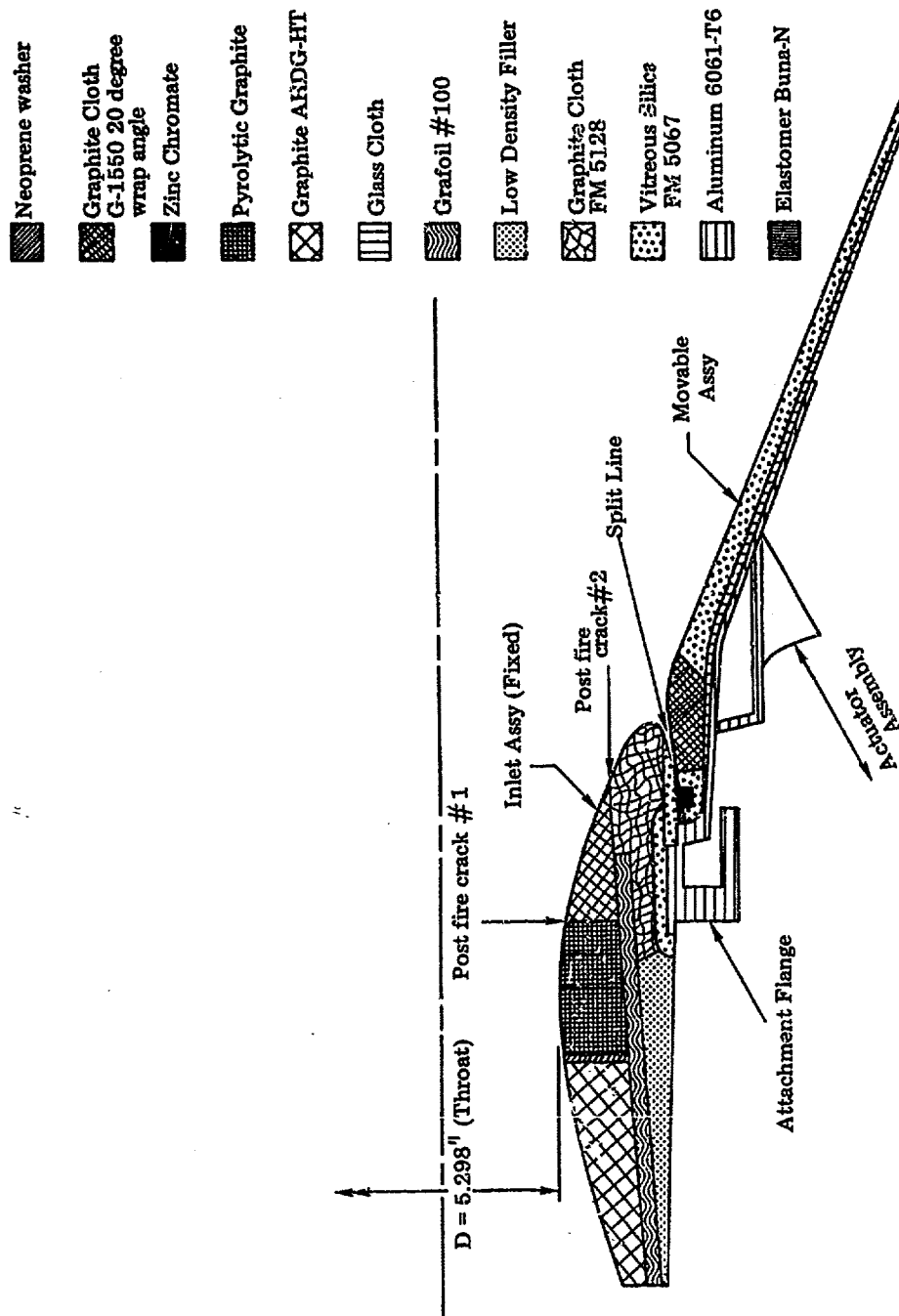


Figure 8. Supersonic Split-line Nozzle Material Description

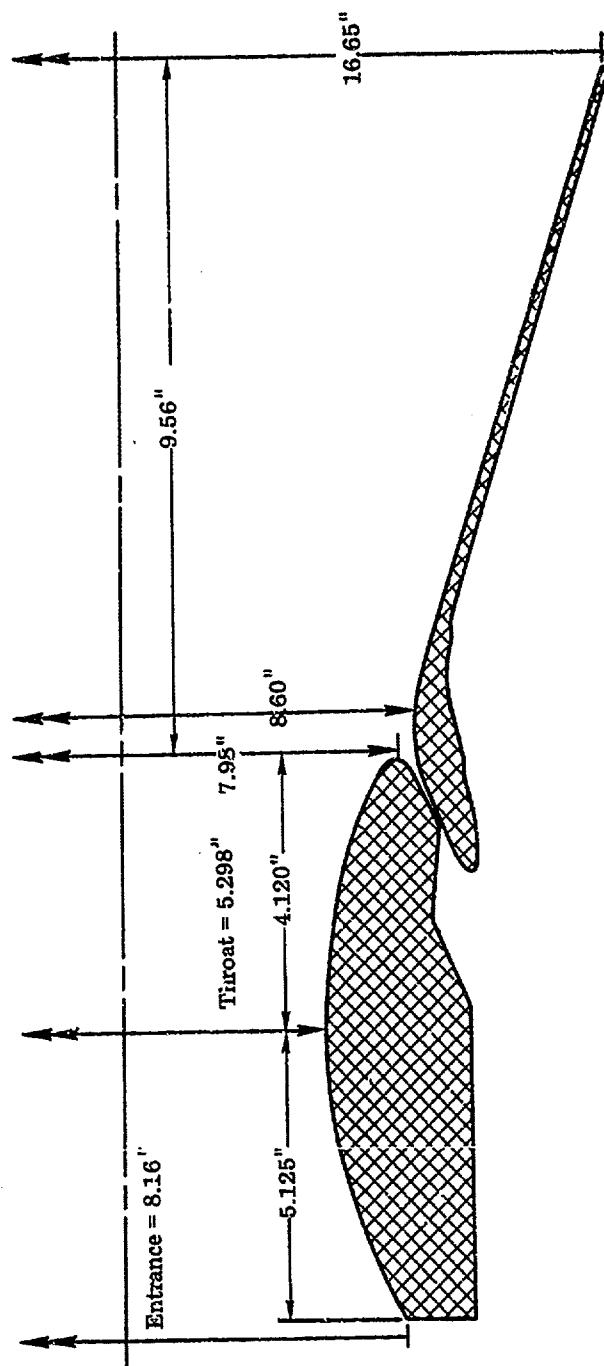


Figure 9. Supersonic Split-line Nozzle Dimensions

the AHDG-HT graphite and the pyrolytic graphite to take up the axial thermal expansion, to prevent loads from being imposed on the relatively brittle materials.

## 2. Movable Assembly

The housing for the movable assembly consisted of a cylindrical section flaring out to a conical shell and was made of 6061-T6 aluminum. The exit cone was primarily silica-phenolic with a fiberglass outer wrap. Graphite cloth (G-1550 Hitco) with a 20 degree wrap angle was used just downstream of the split-line since particle impingement would cause excessive erosion of silica in this region during vectoring.

## 3. Gimbal Ring Assembly

The gimbal ring assembly consisted of a ring and two sets of plain bearings on axes 90 degrees apart. The gimbal ring consisted of a hollow ring with a rectangular cross section, and bearings at two pivot axes located 90 degrees apart. At one axis, the ring was pivoted relative to the stationary inlet assembly and at the other axis, the movable assembly was pivoted relative to the ring. When the nozzle is pivoted about both axes simultaneously, the true motion of the nozzle may be in any desired direction. This action is illustrated in Figure 10. Figure 11 shows the nozzle in the deflected position. The ring was a weldment in which all openings are reinforced with increased section thickness to compensate for local loss of section properties. The ring was designed to limit deflections and satisfactorily carry the loads imposed on it. Excessive deflection of the ring, which would move the movable housing upstream, would tend to reduce clearances in the split-line and possibly increase friction torque. The gimbal ring material was AISI 4130 steel in normalized condition.

## C. ACTUATION SYSTEM

The command signal ( $v_i$  in Figure 5) from guidance was fed into a servo amplifier where it was compared to the signal from the feedback transducer. Any difference between the two signals indicated that the

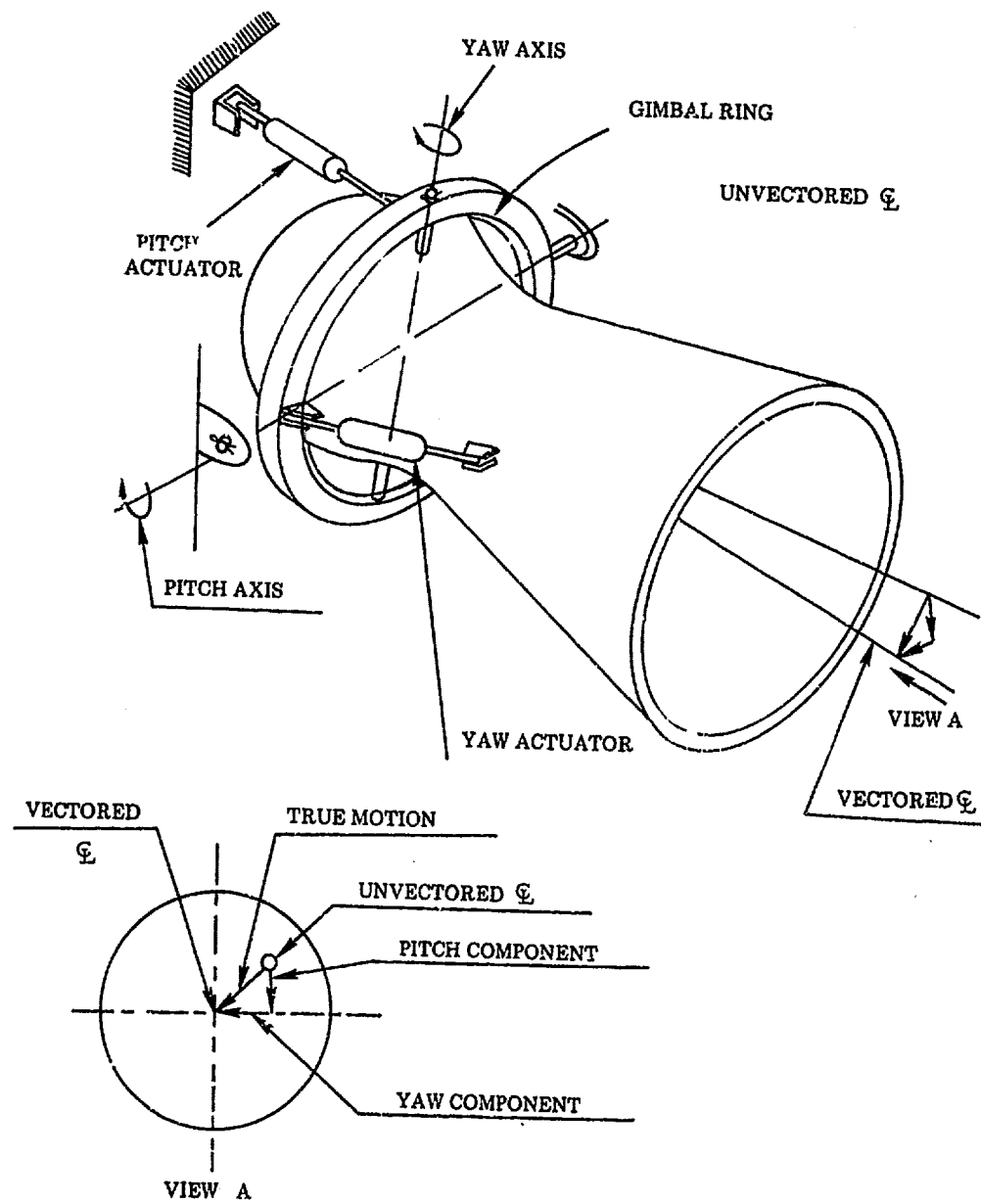


Figure 10. Omniaxis Vectoring With A Gimbal Support

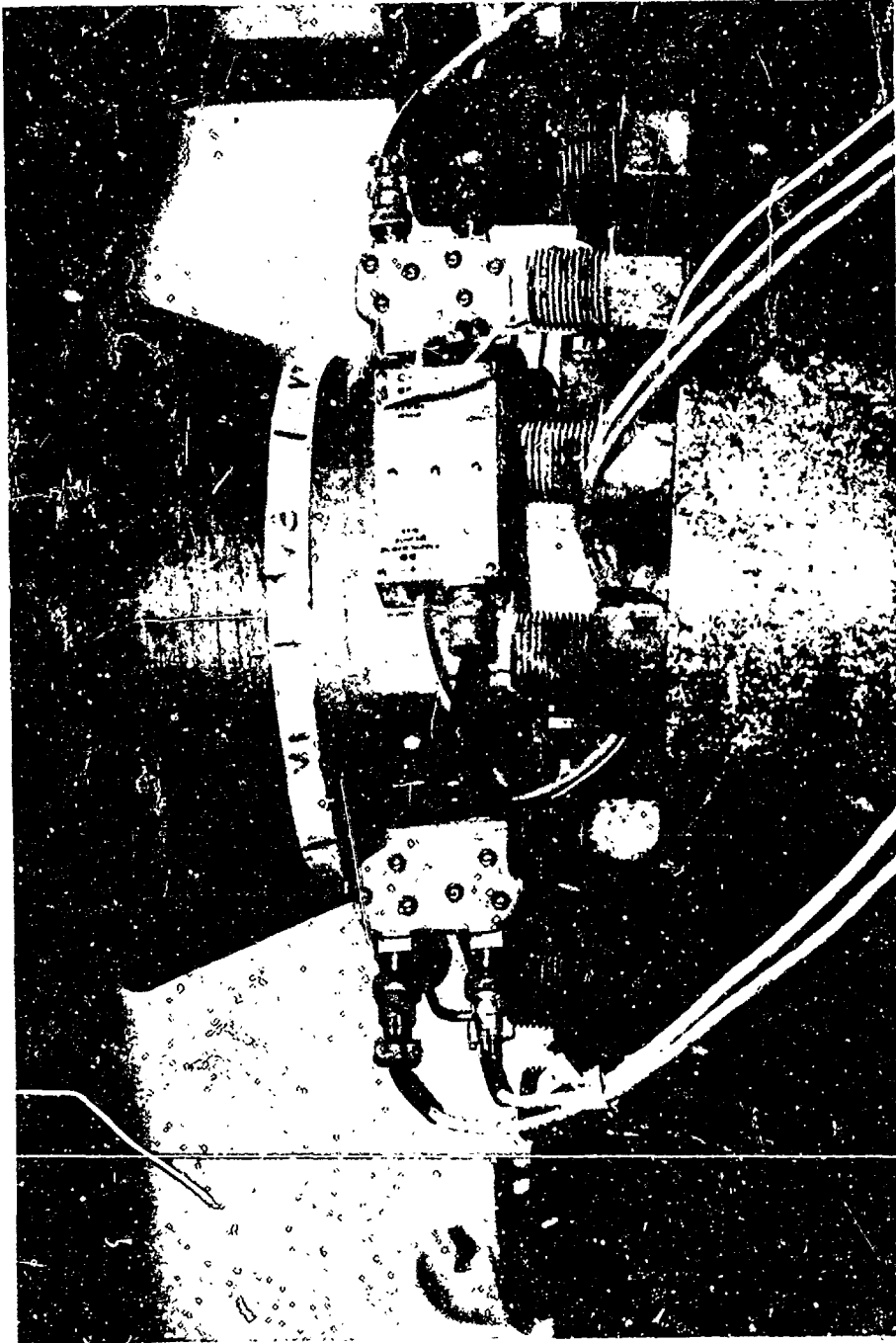


Figure 11. Nozzle in Deflected Position

nozzle was not at the position required by guidance. An error difference signal ( $\epsilon$ ) was generated by the amplifier. The error signal was sent to the servo valve (flow control type) which provided hydraulic oil flow ( $Q$ ) to the actuator proportional to the input current. The direction of the flow to the actuator was determined by the polarity of the error signal, and was intended to reduce the error signal to zero. The pitch and yaw actuators moved the nozzle at a rate proportional to the hydraulic oil flow in the actuator. The servo actuator consisted of a four-way electrohydraulic servo valve, mounted to a balanced-piston double-acting actuator. The pitch and yaw actuators were identical. The servo actuator was designed so that at a constant supply pressure, the velocity of the actuator was proportional to the electrical input signal. The actuator attempted to move the nozzle through an angle ( $\theta_1$ ) toward the command nozzle position. The effective stroke of the actuator was reduced, however, by contact with the nozzle structure. The actual nozzle angle ( $\theta_2$ ) was measured by the feedback transducer which was connected to the swivel trunions and mounted on the gimbal ring. Therefore true nozzle angle was measured. The feedback transducer was a dual element unit, each element of which provided a d. c. voltage signal proportional to the shaft position of the pitch and yaw actuators. One element supplied the feedback signal ( $v_f$ ) to the amplifiers, while the second unit supplied the feedback signal for telemetry. When the feedback signal ( $v_f$ ) equaled the command signal ( $v_i$ ), then the error signal ( $\epsilon$ ) was reduced to zero, the servo valve stopped, and the system was in balance.

## SECTION IV

### AFRPL PROGRAMMER SYSTEM

The Programmer system used in the test firing consisted of the following components:

1. FM reproduce tape system
2. Potentiometer attenuator
3. Dana amplifiers
4. 2 relay configuration circuits

The system was developed to provide remote control (through the automatic firing sequencer) of the preprogrammed command signal for the TVC system. The checkout of the TVC system is described in the Appendix, Section D.

The command signals for the two (pitch and yaw) channels were stored as FM signals on magnetic tape. These FM signals were generated using a digital to analog converter.

The FM signals were converted to dc voltage levels by FM reproduce amplifiers. The dc outputs of the FM reproduce units were amplified by Dana dc amplifiers to provide the required (maximum) signal level of 4 volts. Since the FM reproduce units provided a  $\pm 1$  volt (maximum) dc signal and the minimum gain of the Dana amplifiers was 30, it was necessary to insert a potentiometer attenuator into the circuits, before the Dana amplifiers, to reduce the output to the  $\pm 4$  volts required by the servo amplifiers.

The first relay configuration circuit shorted the input to the Dana amplifier until the tape drive system reached the correct speed. The second



relay circuit shorted the input to the TVC system servo amplifier until the Dana amplifier became stable. The reason for these shorts is discussed in detail in the Appendix, Section D. The system is described with several figures showing the system operation at different times. Figure 12 shows the entire programmer system. Figure 13 shows the system just as the tape system has started to operate. Circuit breaker numbers 1 and 3 are shorted, thus preventing input to the Dana amplifier. Figure 14 shows the system after the tape system has come up to speed. Circuit breaker No. 1 is open and No. 2 is shorted, thus allowing input to the Dana amplifier. No. 3 is still shorted until the Dana amplifier becomes stable. Figure 15 shows the system after the Dana amplifier becomes stable. No. 3 is now open, allowing input to the TVC system servo amplifier.

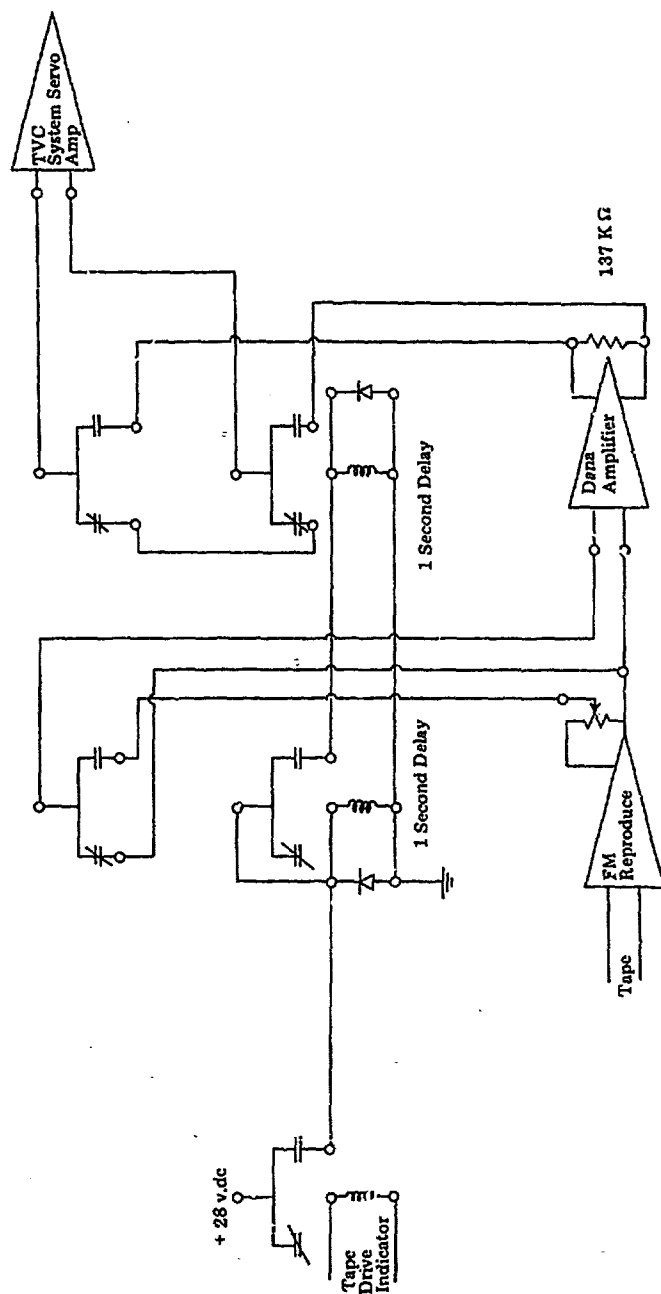


Figure 12. Supersonic Split-line Programmer System

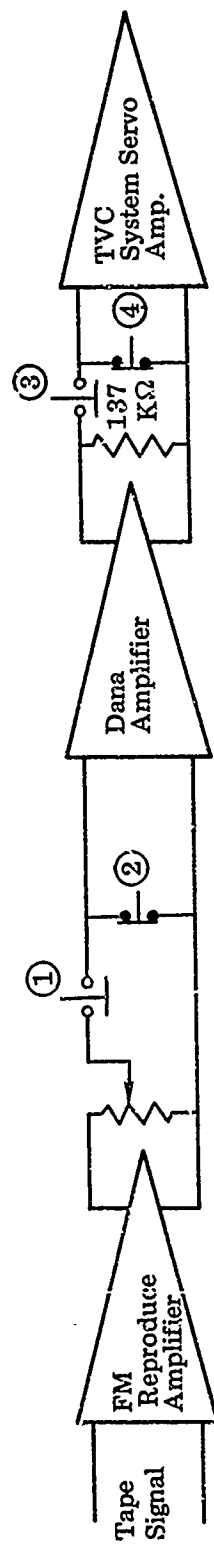


Figure 13. Programmer System State, T = 0 SEC

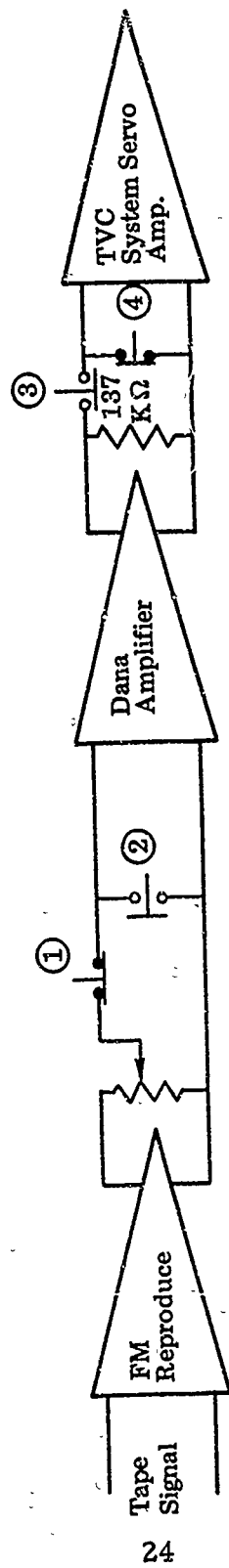


Figure 14. Programmer System State,  $T = 1 \text{ SEC}$

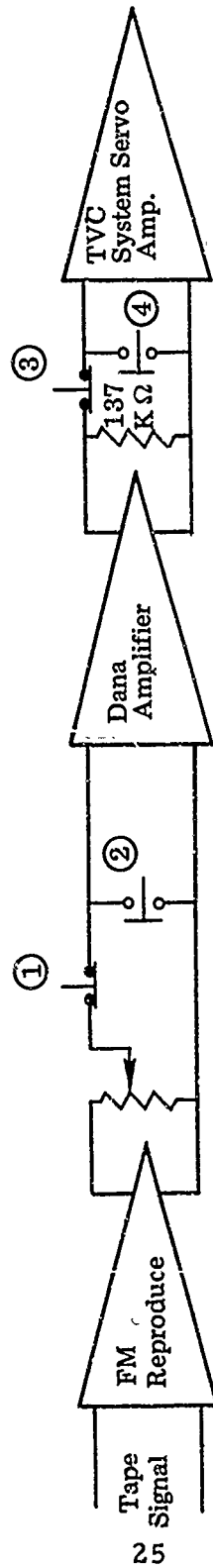


Figure 15. Programmer System State, T = 2 SEC

## SECTION V

### TEST

#### A. EQUIPMENT

##### 1. Thrust Stand

A six-component thrust stand was designed by Gilmore Industries for use with the 84-inch Char motor. The thrust stand was purchased to help fulfill the thrust vector control testing requirements and was used to obtain accurate measurements of axial thrust and side force produced when the TVC system of the nozzle was actuated.

The Gilmore stand is a vertical six-component thrust stand capable of measuring 40,000 pounds of thrust, and side forces up to 5,000 pounds. The stand has an axial load cell and five side force load cells. A calibration was performed on the load cells to determine their individual accuracies. A verification test was conducted, which simulates firing conditions by introducing loads into the thrust stand motor assembly with a secondary load cell acting at the predicted thrust vector action point on the vertical axis. The system accuracy is checked with the accuracy verification. The results showed that the thrust stand was accurate to 0.58 percent and 0.52 percent in the X and Y axis respectively and 0.18 percent in the Z axis (Reference 1). The data from the thrust stand calibration showed that a higher load than was input was being measured. This indicated that a bias error could be present. The X and Y force measurements were consistent throughout the thrust stand calibration. Calculation of side force from X and Y measurements indicated that the side force due to bias was about 1 percent above the input forces. It was necessary to reduce the amount of side force measured during the firing by 1 percent. This was the same as reducing the amplification factor by 1 percent. The thrust stand is shown in Figure 16. A second calibration was performed after the motor was fired, and the thrust stand experienced no measurable calibration changes due to the firing.

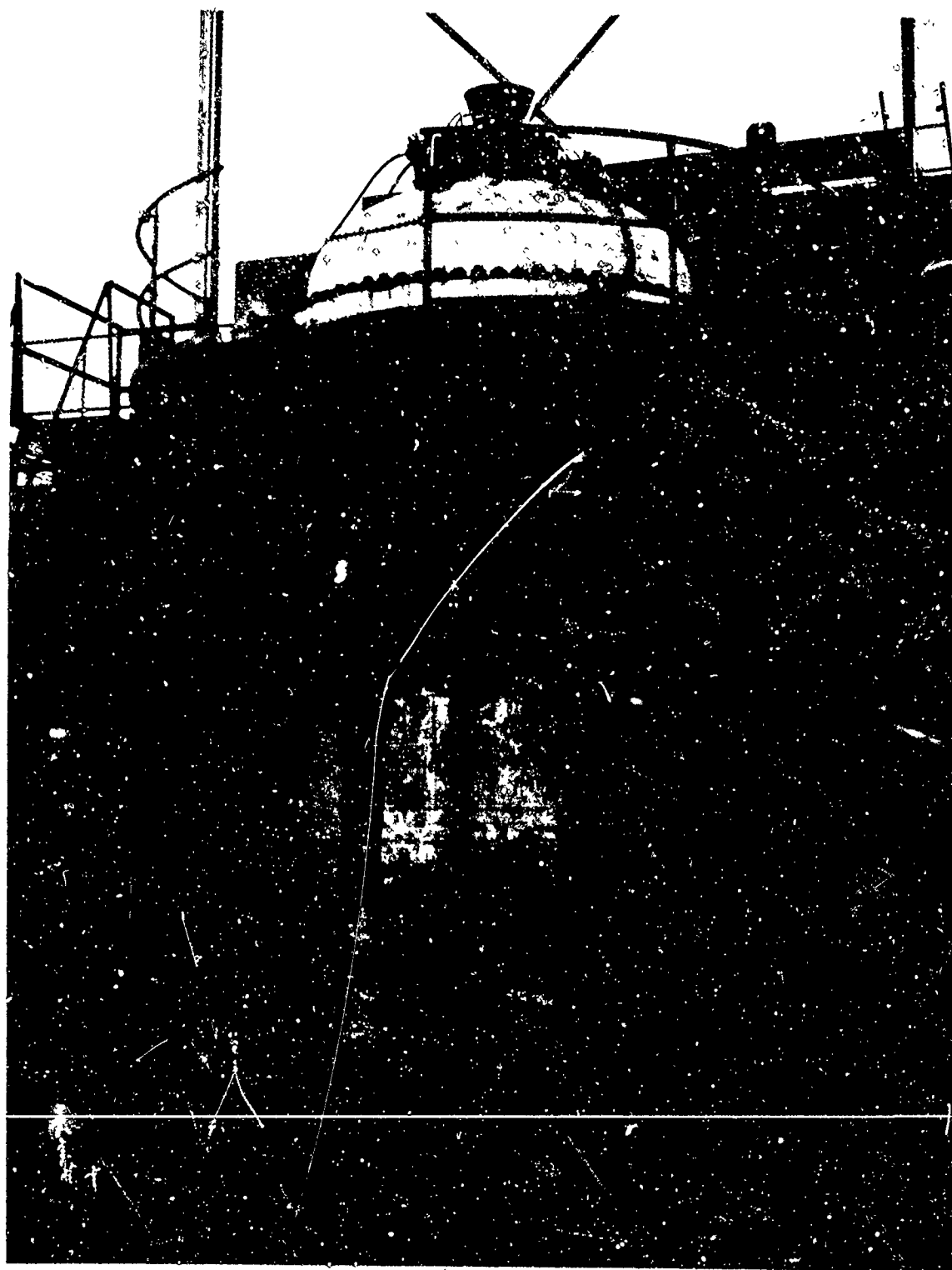


Figure 16. Thrust Stand and Assembled Motor

## 2. Motor

The motor selected to conduct the test firing of the Supersonic Split-Line Nozzle was the 84-inch Char motor shown in Figure 16. This test motor was located at the AFRPL Solid Test Area (1-32), Pad 2. The motor was oriented in a vertical attitude and used uncured propellant in an endburing configuration. This motor was chosen because of its capability to produce 25,000 pounds of thrust for a 40-second duration using an available uncured propellant formulation. The motor has an inside diameter of 77-3/4 inches with a required propellant depth of approximately 10-1/2 inches.

The motor was loaded with approximately 2700 pounds of LPC 614 propellant, (described in the next section) 2 days before the firing. The aft closure was bolted to the top of the motor the day before the firing.

## 3. Propellant and Igniters

The propellant used for this test was manufactured by the Lockheed Propulsion Company, Redlands, California and was designated LPC-614. This is one of a family of uncured propellant formulations employed by the AFRPL for rocket motor hardware evaluation. The propellant composition contained 16 percent aluminum and conventional percentages of ammonium perchlorate hydrocarbon binder and ferric oxide (burn-rate modifier). The propellant was ignited with pancake igniters (propellant surface ignition) and a single Lockheed pyrogen igniter (chamber pressure buildup) mounted on the aft closure (Figure 17). The significant ballistic properties of the propellant at 700 psi chamber pressure were:

- |                            |             |
|----------------------------|-------------|
| 1. Flame Temperature       | 5744°F      |
| 2. Characteristic velocity | 5184 ft/sec |
| 3. Molecular Weight        | 28.265      |
| 4. Specific Heat ratio     | 1.189       |



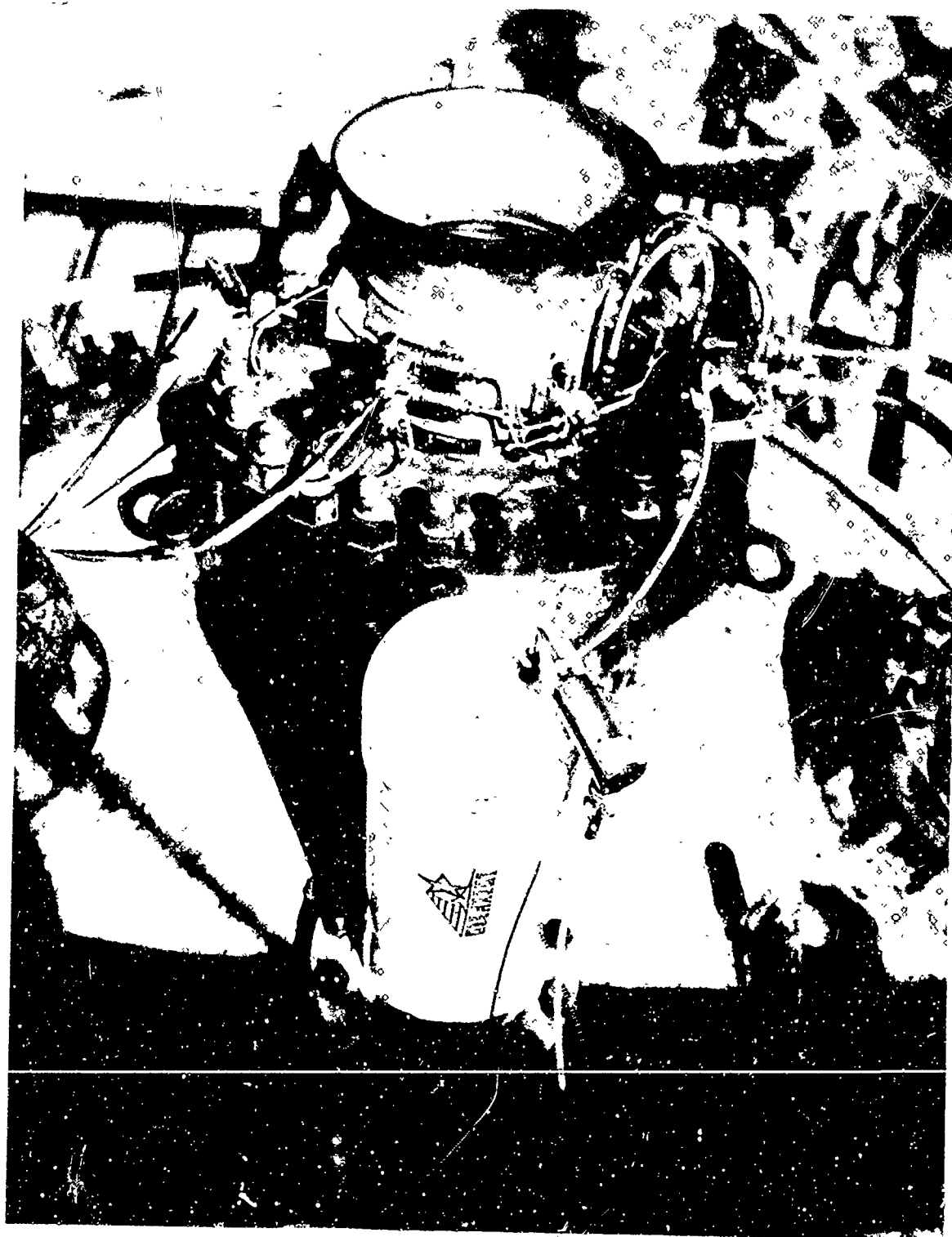


Figure 17. Pyrogen Igniter on Motor

## B. FIRING

The firing of the supersonic split-line nozzle on the 84-inch Char motor took place on 29 January 1969. The final checkout of the nozzle was conducted approximately 1-1/2 hours before the firing to verify that all instrumentation was functioning properly. A smooth ignition was produced after a 1/4-second delay, which was considered excellent for the large motor free volume of approximately 400,000 cubic inches. Desired test conditions were 38 seconds duration and maximum  $P_c = 560$  psi. The actual duration was 35 seconds, and the maximum pressure was about 660 psi with an average of 640 psi. The pressure curve was very flat and started to tail off at about 36 seconds, as can be seen in the pressure trace, Figure 24. The difference between actual and predicted conditions was attributed to unreliable propellant burn-rate data used for making the predictions.

## C. NOZZLE POSTTEST CONDITION

The nozzle survived the firing very well with minimal erosion in the throat. The prefire throat diameter was 5.298 inches and the postfire diameter was 5.340 inches. The erosion rate was 0.625 mils per second for a duration of 35 seconds. Figures 18, 20, and 21 show the condition of the nozzle before and after the firing. It can be seen that there was local erosion downstream of the nozzle throat. This is typical of nozzle performance downstream of a pyrolytic graphite washer throat. The split-line gap had evidence of local erosion in the pitch plane. This could explain the increased amount of friction mentioned later in the report. The high-speed motion picture films of the firing indicated that a large amount of Grafoil No. 100 was ejected from the nozzle. This probably was caused by two cracks in the nozzle, as shown in Figure 8. Higher pressure at crack number one apparently caused a large amount of Grafoil to be ejected at crack number two, which was at a lower pressure. Figure 22 shows that the entrance section of the nozzle was somewhat charred. This charred region consisted of the V-61 insulation which was used to form the contour from the aft closure to the nozzle entrance section. During the postfire

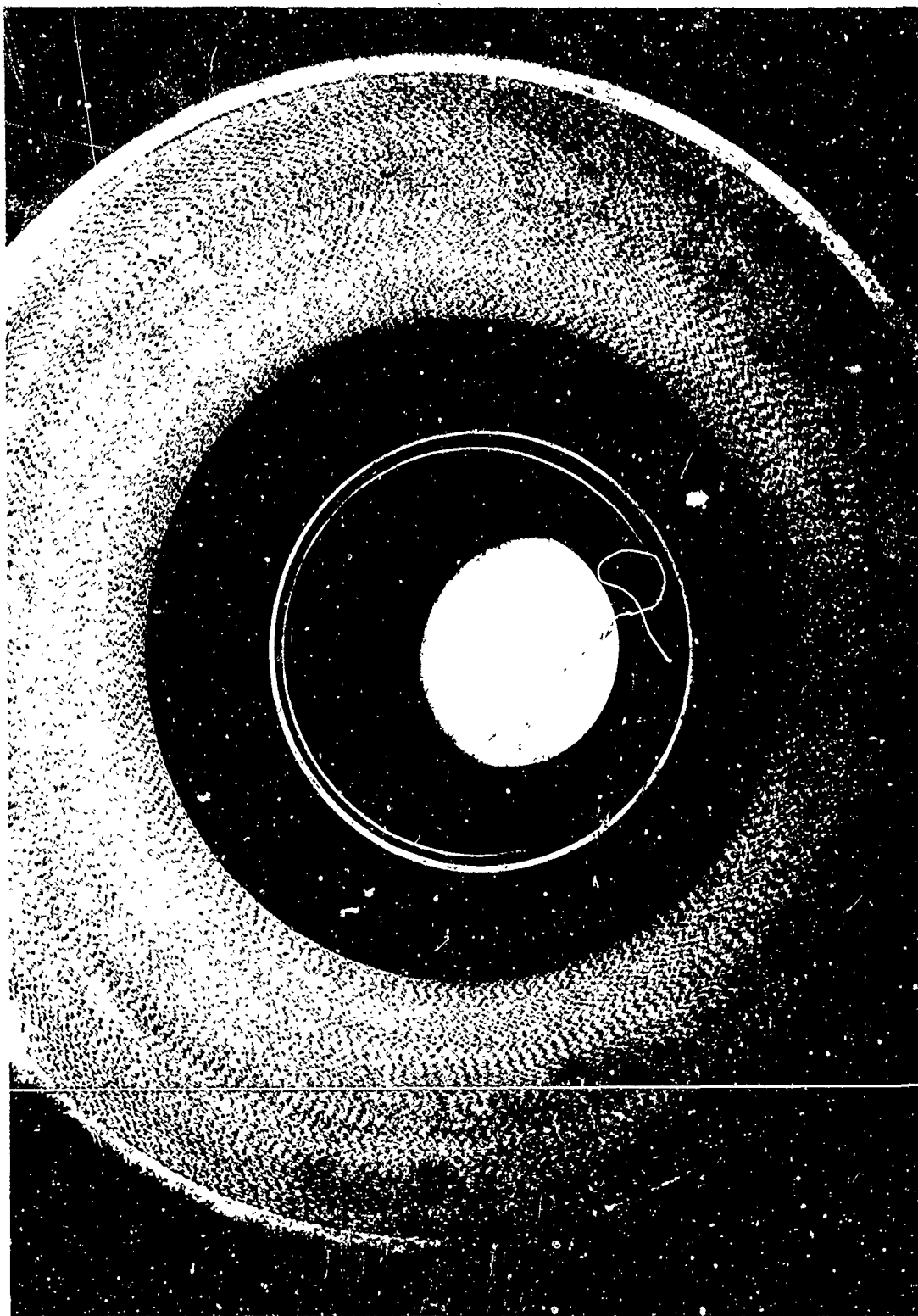


Figure 18. Top of Nozzle, Prefire

examination of the nozzle, the exit cone came off while the nozzle was being manually moved to determine how much friction was present. The point where the exit cone came off is shown in Figure 19. Very little force was required to separate the exit cone because of material strength degradation which occurred during heat soak after the firing.

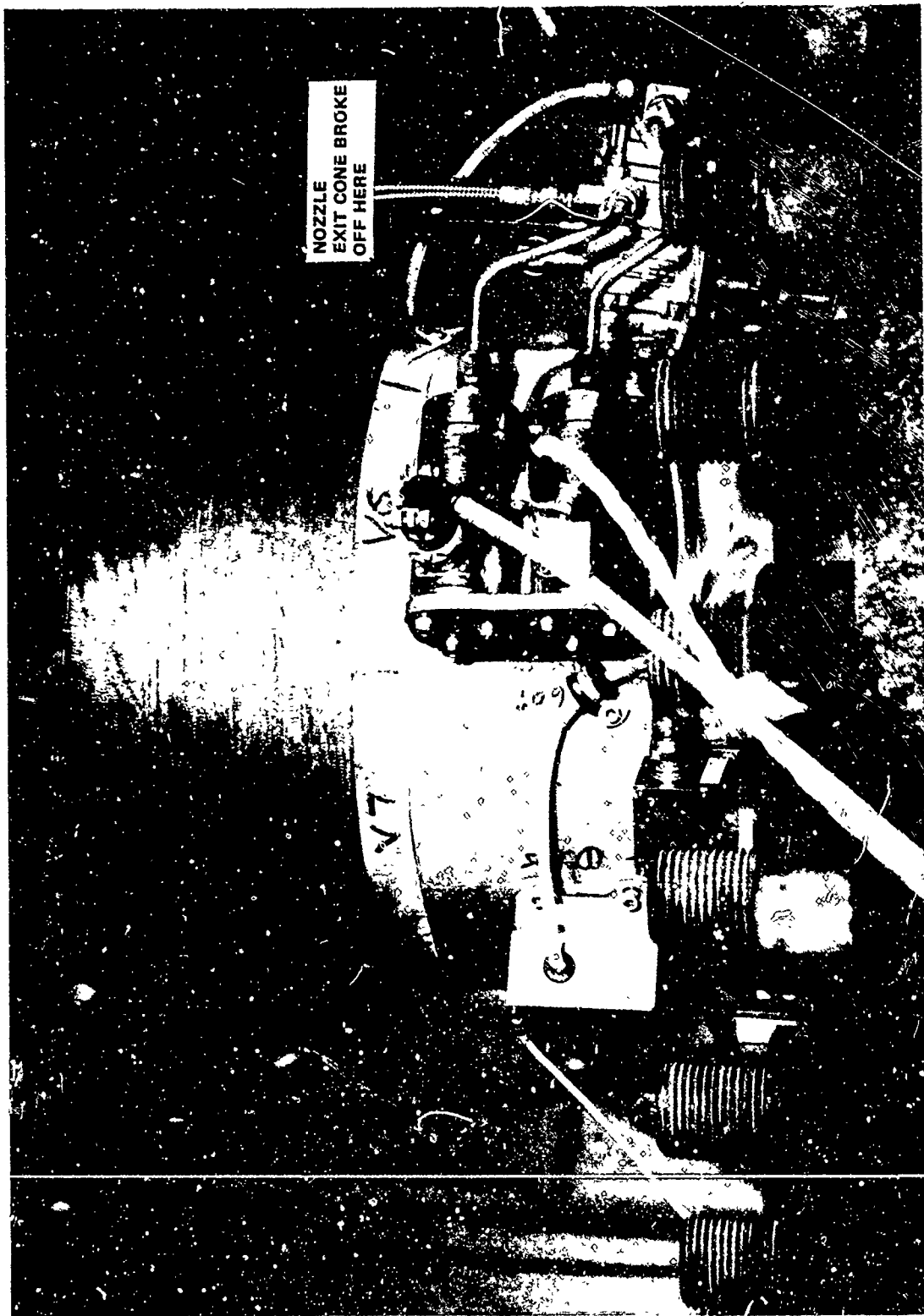


Figure 19. Postfire Nozzle, Side View



Figure 20. Postfire Nozzle, Top View



Figure 21. Postfire Nozzle, Top View



Figure 22. Postfire Nozzle, Bottom View



## SECTION VI

### TEST RESULTS

#### A. DATA REDUCTION

The digital tape readings were transformed into engineering units for the following items:

1. Chamber pressure PC1 and PC2 (psi)
2. Load cell outputs  $X_1$ ,  $X_2$ ,  $X_3$  (lbs)
3. Load cell outputs  $Y_1$ ,  $Y_2$  (lbs)
4. Load cell outputs Z (lbs)
5. Hydraulic pressure in the pressure feed system HYPD (psi)
6. Yaw pressure extend YAWP (psi)
7. Yaw pressure retract YAWR (psi)
8. Pitch pressure extend PP (psi)
9. Pitch pressure retract PR (psi)
10. Yaw signal volts YAWSV
11. Yaw signal counts YAWSC
12. Pitch signal volts PSV
13. Pitch signal counts PSC
14. Yaw output volts YAWOV
15. Yaw output counts YAWOC
16. Pitch output volts POV
17. Pitch output counts POC

In order to initiate the data analysis, the sum of  $X_1$ ,  $X_2$ ,  $X_3$ , the sum of  $Y_1$  and  $Y_2$ , and the corrected Z force were computed. The propellant burn rate was calculated from the pressure trace, depth of propellant and density. The force measured by the Z load cell included the instantaneous weight of the propellant that remained in the motor. All load cells had been adjusted to "zero out" tare weights before the firing, so a propellant flow-rate correction was required. The computer took the changing tare weight into account by adding the amount of propellant that was burned during an incremented time as follows:

$$\text{Weight of propellant at any time } t = (W_{pT})$$

where:

$$W_{pT} = \text{burn rate} \left( \frac{\text{lbs}}{\text{sec}} \right) \times \text{time (sec)} = \text{lbs}$$

$$\text{Corrected thrust at anytime } t = Z \text{ (force read by load cells)} + W_{pT}$$

or

$$FZCOR = Z + W_{pT} \text{ (lbs)}$$

The torque required to actuate the TVC system was computed. From the geometry of the nozzle, the torque required was:

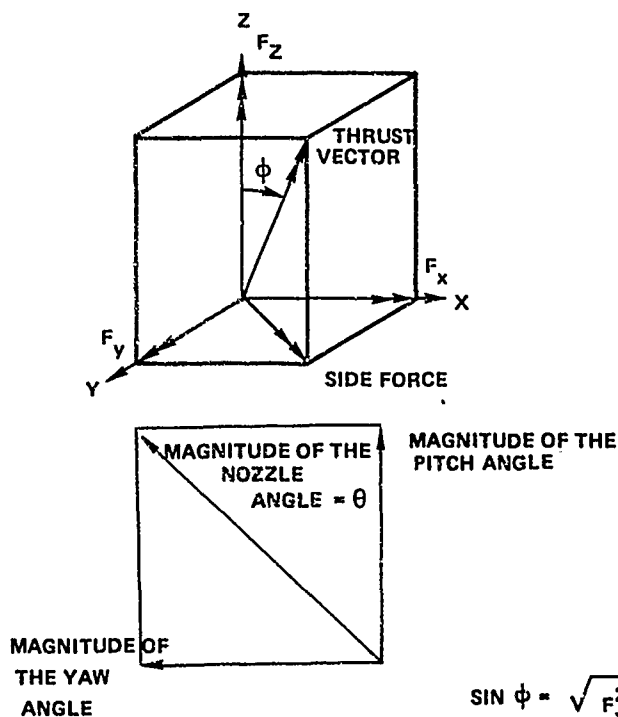
$$T_{YAW} = 5.183 (YAWP - YAWR) \text{ in-lbs}$$

$$T_{PITCH} = 5.183 (PP - PR) \text{ in-lbs}$$

This equation is derived in the Appendix, Section B.

Amplification factor is the ratio of the thrust vector angle to the actual nozzle position angle.

$$\text{AMF (amplification factor)} = \frac{\text{angle of thrust vector}}{\text{angle of nozzle}} = \phi / \theta$$



$$\sin \phi = \frac{\sqrt{F_x^2 + F_y^2}}{\sqrt{F_x^2 + F_y^2 + F_z^2}} \quad \frac{\text{RADIANS} \times 57.3 \text{ DEGREES}}{\text{RADIAN}}$$

$$= \phi \text{ FOR SMALL ANGLES LESS THAN } 6^\circ$$

$$\theta = \sqrt{\text{Pov}^2 + \text{Yaw ov}^2} \text{ which is measured in volts}$$

$$\text{Thus, AMF} = \frac{\sqrt{F_x^2 + F_y^2}}{\sqrt{F_x^2 + F_y^2 + F_z^2}} \times \frac{57.3}{\sqrt{\text{Pov}^2 + \text{Yaw ov}^2}}$$

The following data items were machine plotted: Only the plots that are numbered below are shown in the Appendix, Section E.

1. Chamber pressure versus time	PCI versus time Figure 37
2. Corrected thrust versus time	FVCORA versus time Figure 38
3. Sum of $X_1$ , $X_2$ , $X_3$ versus time	SUM X versus time Figure 39
4. Sum of $Y_1$ and $Y_2$ versus time	SUM Y versus time Figure 40
5. Nozzle Pitch angle versus time	Pitch versus time
6. Nozzle Yaw angle versus time	Yaw versus time
7. Torque (yaw) versus time	TorYAW versus time Figure 41
8. Torque (pitch) versus time	TorP versus time Figure 42
9. Yaw output volts versus time	YAWOV versus time Figure 43
10. Yaw input volts versus time	YAWSV versus time
11. Yaw output counts versus time	YAWOC versus time
12. Yaw signal counts versus time	YAWSC versus time
13. Pitch output volts versus time	POV versus time Figure 44
14. Pitch input volts versus time	PSV versus time
15. Pitch output counts versus time	POC versus time
16. Pitch input counts versus time	PSC versus time
17. Amplification factor versus time	AMF versus time

Some of the graphs exhibited minimal noise from the digital system and an acceptable amount of ringing in the thrust stand. But some plots, mainly those which were produced by the use of equations relating original data, showed considerable variation from point to point. This data was "smoothed" by taking the average of all the points and plotting a new graph. These new plots were then used to evaluate the performance of the TVC system. An example of a plot before and after this "smoothing" process can be seen in the original plot (Figure 25) and the new plot (Figure 40) of Sum Y versus time.

## B. DATA INTERPRETATION

As stated in the previous section, some of the data obtained was "noisy." Thus, new curves were hand plotted reducing the "noise" to a minimum. A step-by-step evaluation of the smoothed data utilized for the TVC performance evaluation is given below.

1. The amplification factor was determined by the equation:

$$AMF = \frac{\sqrt{F_x^2 + F_y^2} \times 57.3}{\sqrt{F_x^2 + F_y^2 + F_z^2}} \sqrt{(P \text{ angle})^2 + (YAW \text{ angle})^2}$$

From the plot of  $F_z$  (axial thrust) versus time, Figures 23 and 38, it can be seen that the thrust reached a steady-state level of about 21,000 pounds at about 6 seconds. The limited amount of steady ringing shown in the curve indicated that thrust at any time could be determined with an acceptable small error.

The plot of  $F_x$  versus time (Figure 26) did not exhibit much "ringing" except at the very beginning of the firing. The value of  $F_x$  at any time did not impose a problem because the curve required very little "smoothing".

The plot of  $F_y$  versus time indicated that the ringing level was considerable. This was attested to by the fact that the value of  $F_y$  during the first 4 or 5 seconds of the firing varied from 100 to 500 pounds. When the nozzle was not being actuated during the duty cycle, the Y side force fluctuated as much as 250 pounds from the anticipated steady-state value. The Y side force plot (Figure 25 and 40) was "smoothed" to allow better interpretation of the data. The nozzle pitch and yaw angular positions were used to help smooth the  $F_y$  curve. The periods during which the nozzle was not being actuated should have resulted in no change in Y side force. During these periods, the Y side force seemed to reach steady state except for the ringing. The final value of  $F_y$  did not go back to zero load, but

settled at approximately 100 pounds. Several things could have caused this bias. The  $Y_1$  load cell was connected to an iron A frame which was not as sturdy as the concrete wall to which the  $X_1$  and  $X_3$  load cells were connected. The motor could have been misaligned in the thrust stand in the Y direction. Calculations showed that with a motor weight of approximately 20,000 pounds, a side force of 100 pounds could be caused by an angular misalignment of only  $1/3$  degree. Also, considerable noise in the Y load cell feedback channel resulted from a malfunctioning Dana amplifier.

There was very little noise in the pitch and yaw output voltages (Figures 43 and 44) which indicated that the actual angular position of the nozzle was accurately known at all times. The digital system was set up to record 1 volt as one degree and 4 volts as 8000 counts. Before the firing, a calibration was performed to determine what voltages the pitch and yaw transducers were actually receiving. These values during the calibration are shown below:

	ZERO POSITION	MAXIMUM DEFLECTION	MAXIMUM TRAVEL CORRECTING FOR ZERO SHIFT
Pitch	473.94 counts	-7257.40 counts	7731 counts
Yaw	598.54 counts	-7197.48 counts	7796 counts

Thus, the nozzle did not actually travel 4 degrees. Since the output voltage was based on 4 degrees per 8000 counts, the actual voltage was corrected as shown below:

$$\text{PITCH ANGLE} = \frac{7731}{8000} \times \text{POV} = 0.966 \times \text{POV} \quad \text{degrees}$$

$$\text{YAW ANGLE} = \frac{7796}{8000} \times \text{YAWOV} = 0.975 \times \text{YAWOV} \quad \text{degrees}$$

### 1. Amplification Factor

An accurate amplification factor could be calculated only for cases where considerable side force was being developed, and where the nozzle was in a steady state position. From Figure 27, nozzle angle versus time, 10 time periods were taken to calculate the amplification factor. The calculation of the amplification factor for position number one is shown below with all subsequent values listed in Table I. The calculations were done for the actual nozzle angle.

$$AMF = \frac{\sqrt{F_x^2 + F_y^2} \times 57.3}{\sqrt{F_x^2 + F_y^2 + F_z^2}} \sqrt{P^2 \text{ angle} + Y \text{ angle}^2}$$

From Figure 28 side force,  $F_x^2 + F_y^2 = 541 \text{ lbs}$

From Figure 23 thrust vector,  $F_x^2 + F_y^2 + F_z^2 = 21,200 \text{ lbs}$

From Figure 27 actual nozzle angle,  $P^2 + Y^2 = 1.0 \text{ degrees}$

$$AMF_1 = \frac{541 \times 57.3}{21200 \times 1.0} = 1.46$$

It can be seen that amplification factors 1 and 8 are high relative to the other values. This was caused by side force that was present while the nozzle was at zero angular position, probably induced by thrust-stand misalignments. Although the side force preload was accounted for by subtracting it out during calculations, the side force which built up as the thrust increased could not be considered because of its lack of definition. When the nozzle went to zero angular position the side force would return to values ranging from as much as 250 pounds to as little as 20 pounds, and many values in between as can be seen in Figure 28 (side force). As the nozzle angular position increased, the effect of the initial side force on amplification factor calculations decreased. Since the effect of the side force preload upon the amplification factor was not known, an average of the 10 amplification factors was taken. The average was 1.15 with a

TABLE I. AMPLIFICATION FACTOR

CASE	SIDE FORCE (LBS)	THRUST VECTOR MAGNITUDE (LBS)	NOZZLE ANGLE (DEGREES)	AMPLIFICATION FACTOR
1	541	21200	1.0	1.46
2	840	21200	1.96	1.16
3	1165	21100	2.93	1.09
4	1485	21000	3.92	1.04
5	1467	21000	3.90	1.03
6	1125	20900	2.94	1.04
7	796	20800	1.96	1.11
8	530	20800	1.02	1.42
9	1920	20800	*5.06	1.04
10	1660	20700	4.07	1.12

\*Yaw and pitch were actuated simultaneously such that nozzle angle<sup>2</sup> = pitch angle<sup>2</sup> + yaw angle<sup>2</sup>.

$\sigma$  of 0.16. Leaving the two high values (1 and 8 from Table I), gives an average of 1.08 with a  $\sigma$  of 0.05. This was the most reasonable value, and was used in determining nozzle performance.

## 2. Actuation Torque

The actuation torque required to move the nozzle against the aerodynamic forces was given by

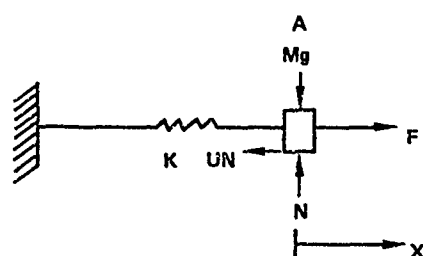
$$\text{Torque Yaw} = 5.183 (\text{Yaw P} - \text{Yaw R}) \text{ in-lbs}$$

$$\text{Torque Pitch} = 5.183 (\text{PP} - \text{PR}) \text{ in-lbs}$$

These equations are derived in the Appendix, Section B.



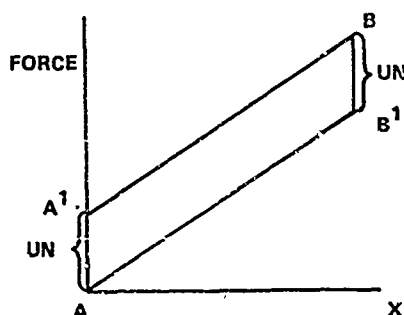
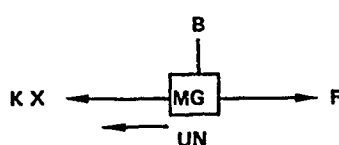
Pitch and yaw torque versus time curves, Figures 30 and 33, were acceptably smooth as recorded. From these torque curves, along with the actual pitch and yaw angle plots, an angle versus torque curve was constructed (Figures 31 and 34). If Figures 31 and 34, pitch and yaw actual angle versus torque, the curves are labeled to define actuation direction. The up-down label and points 1-2-3-4 show where the data was taken from on the 3 pitch and 3 yaw curves, Figures 29 to 34. As can be seen in the angle versus torque curves, considerable hysteresis was present. The area between the two curves was the work done against friction in moving the nozzle during the static firing. The reason for this can be seen in the following analogy. Consider a spring mass system with friction.



$\mu$  = Coeff. of static friction

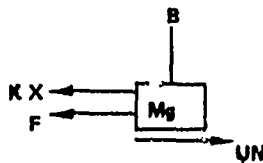
$N$  = Normal force

$K$  = Spring constant



Moving the mass in the positive X direction gives  $\Sigma F_x = 0$   $F = Kx + \mu N$   
Thus, to move a distance from A to B, the Force must first overcome the initial frictional force.

Going from B to A after the mass has stopped, the Force must overcome the force of friction but in the opposite direction.



$$\sum F_x = 0 \quad F + Kx = \mu N$$

$$F = \mu N - Kx$$

Thus, the work done against friction is

$$\int_A^B F dx + \int_B^A F dx = \text{area inside curve}$$

The units are Force X Length = in-lbs.

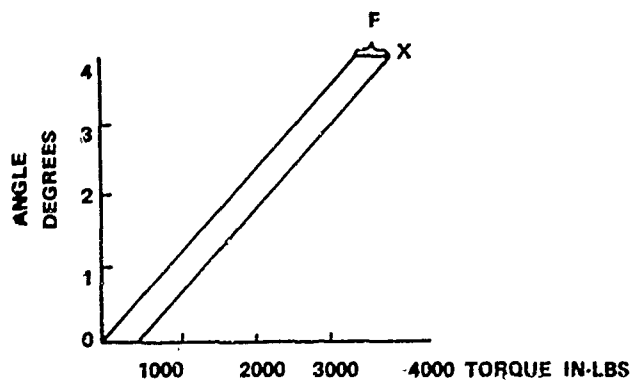
The F versus X curve is analogous to the angle versus torque curve except for the following:

(1) The Force on the spring system is analogous to the actuation torque on the nozzle. Their difference is in the units used.

(2) The X direction in the spring mass system is equivalent to the pitch or yaw angle axis, except the angle units are in radians.

The area inside the angle-torque curve is equal to in-lb-radians or in-lb of work. Determining the amount of small sections inside the curves was used to determine the area inside the curves. The area inside the curve was multiplied by a conversion factor of 2.5 in-lb-degree/section<sup>2</sup>. The result of this is shown in Table II.

The amount of frictional torque present is analogous to B-B' or A-A' on the spring-mass system sketch.



The amount of frictional torque present is equal to the length F on the above diagram. The point X can be determined knowing the area inside the curve and the 2 axes intercepts of point X. The position of X is shown on the two angle versus torque plots. The calculation of F is shown in the Appendix Section A and Table II shows these values. The positions are labeled on Figures 31 and 34 to show where the data was taken from.

The area under the curves and the results are shown in Table II.

From Figures 31 and 34, angle versus torque, it can be seen that as the nozzle reaches about 3-1/2 degrees, the amount of torque required to deflect the nozzle increased. Figure 31 shows that about 2000 in-lb of torque is applied to the nozzle resulting in very little nozzle rotation. The same can be seen in Figure 34. A probable cause of the increase was increased friction resulting from the split-line gap being opened significantly, causing local erosion in that area. Particles could have entered the seal region, thus increasing the amount of friction. An accumulation of particles could have caused the nozzle to stop moving, although the actuator was still applying a force to the nozzle trying to make it move more. Postfire analysis of the nozzle showed that there was local erosion in the throat which could have contributed to the friction problems (Figure 20). As the nozzle moved in the opposite direction, these particles were probably ejected from the seal region, resulting in less friction. Figures 31 and 34 show that the curves are essentially parallel from 0 to 3 degrees on both up and down cycles which indicates that torque was a linear function of nozzle angle. The frictional forces present at the tail of each nozzle cycle can be accounted for by subtracting them out. This resulted in reasonable values of torque required to actuate the nozzle through the duty cycle. Revised friction torque is shown in Table IV.

TABLE II. FRICTION WORK

POSITION	AREA BETWEEN CURVES	WORK DONE AGAINST FRICTION (in-lb)	TOTAL WORK	AERO WORK = TW-FW	FRICTION WORK TOTAL WORK
P <sub>1</sub>	348	870	5910	5040	.147
P <sub>2</sub>	495	1237	11263	10026	.109
Y <sub>1</sub>	313	783	9907	9124	.086
Y <sub>2</sub>	260	650	11965	11315	.054
Average .0990					

Friction work/total work shows that the amount of work required to offset frictional forces was small, on the average of less than 10% of total.

TABLE III. FRICTION TORQUE

POSITION	FRICTION TORQUE (F'T)	TOTAL TORQUE (TT)	AERO TORQUE	FRICTION TORQUE TOTAL TORQUE
P <sub>1</sub>	181.25 in-lb	2800 in-lb	2618.75	.0646
P <sub>2</sub>	191.12 in-lb	4650 in-lb	4458.88	.0411
Y <sub>2</sub>	106.55 in-lb	5000 in-lb	4893.45	.0213
Y <sub>1</sub>	139.98 in-lb	4400 in-lb	4260.02	.0318
Average .0397				

Friction torque/total torque as shown in Table III also indicates that the amount of torque required to overcome friction is less than 4% of the total torque.

TABLE IV. REVISED FRICTION TORQUE

POSITION	TOTAL TORQUE	MAX ANGLE	FRICT. TORQUE	AERO TORQUE	AERO TORQUE in-lb DEGREE deg.
P <sub>1</sub>	2800 in-lb	3.92°	223	2577	657
P <sub>2</sub>	2700 in-lb	3.40°	353	2347	690
Y <sub>1</sub>	3100 in-lb	3.9	192	2908	745
Y <sub>2</sub>	3500 in-lb	3.75	100	3400	907

This revised chart shows that the aerodynamic torque in the yaw plane was considerably higher than in the pitch plane. It was impossible to accurately determine the values for Table IV.

The torque values for  $P_1$  are the most accurate because there was no additional friction as compared to the other cycles which encountered friction. From Figure 31, pitch versus torque, the slope of cycles 1 and 2 are almost parallel as shown by the indicated line. The cycle 2 slope is different because of the uncertainty in determining where the additional friction comes into effect. The problem of determining the cutoff point for pitch cycle 2 was difficult. This point (8A on Figure 31) was chosen as the point where the nozzle did not move although there was an increase in torque. In Figure 34, yaw versus torque, the cutoff point for cycle one was chosen as Point 3A because of a discontinuity in the curve there. The nozzle was slipping with no addition of torque, which implied that at this location the duty cycle was to stop. Point 4A was determined as the cutoff mark for cycle 2 of yaw in the same manner as Point 8A on pitch cycle 2 was determined.

Thus, the most accurate value of torque was exhibited in cycle 1 of pitch. 2800 in-lb of torque was required to actuate the nozzle 3.92 degrees. This corresponds to an aerodynamic spring rate of about 657 in-lb/degree. The highest value was about 3500 in-lbs, which was an increase of about 25% over 2800 in-lbs.

### C. DATA EVALUATION

The force amplification factor that was obtained varied by as much as 40% when taken at different times during the duty cycle. As mentioned earlier, this was caused by a side force preload in the nonactuated position. Neglecting the unrealistic amplification factors resulted in a more reasonable value of 1.08 with a variance of about 5% in either direction. A subsonic split-line nozzle (Amplification Factor = 1.0) would produce a side force of 1855 pounds or less for a 5-degree deflection with 21,200 pounds of axial thrust, compared to 2020 pounds for a supersonic split-line nozzle. Thus, for the same angle, the SSSL nozzle produced about 8% more side force.

The amount of torque required to actuate the nozzle through the programmed duty cycle varied when calculated at several different times. A reasonable value to actuate the nozzle through  $3.92^\circ$  was determined as 2800 in-lb with about 220 in-lb of this being required to overcome friction. The maximum torque required to actuate the nozzle was 5000 in-lb as shown in Table III. Thus, at least 5000 in-lb of torque was available in the actuators which was far more than it took to actuate the nozzle. The performance of the actuators was excellent based on their satisfying power requirements.

The thrust stand performed satisfactorily although there was a large amount of dynamic ringing in the Y axis of the stand. The X axis side force plot (Figure 39) shows that there was an insignificant amount of ringing or "noise" except at the beginning of the firing when the thrust was increasing. During the firing, the X plot was essentially parallel to the actual nozzle position plot which indicated that the thrust stand could distinguish when the nozzle was being actuated and when it was not, with very little lag time. The accuracy of the thrust stand to measure side force had been determined in another report as about 0.5% of point. As stated earlier, the dynamic ringing that was in the side force plots was "smoothed" to reduce this possible source of error in the determination of the amplification factor.

The amplification factor was determined to be about 1.08 with a  $\pm$  error of about 5.5%. The error was determined by adding the variance in the amplification calculation (5.0%) to the thrust stand error (.5%). Correcting by bias, (-1%) this reduced to about  $1.07 \pm 5.5\%$ .



## SECTION VII

### CONCLUSIONS AND RECOMMENDATIONS

#### A. CONCLUSIONS

1. The supersonic split-line concept was demonstrated by the measurement of an amplification factor greater than 1.0.
2. The Arde Portland supersonic split-line nozzle design performed satisfactorily producing an amplification factor of 1.08. Only 2800 in-lb of torque was required to actuate the nozzle in three out of four of the duty cycle steps investigated during the firing.
3. Irregular split-line erosion was experienced with increased actuation friction as a result.
4. The performance of the 84-inch Char motor was excellent.
5. The performance of the Gilmore thrust stand was excellent.

#### B. RECOMMENDATIONS

1. The supersonic split-line nozzle concept should be considered when a TVC system is needed.
2. A detailed postfire analysis of the test nozzle should be conducted to examine in depth material degradation and its effect on nozzle performance. Emphasis should be placed on determining if erosion rates in the pitch and yaw planes were higher than usual.
3. Advanced large nozzle (5-10 inch throat diameter) TVC systems should be tested on the 84-inch Char motor because the thrust stand gives results that are accurate and predictable.

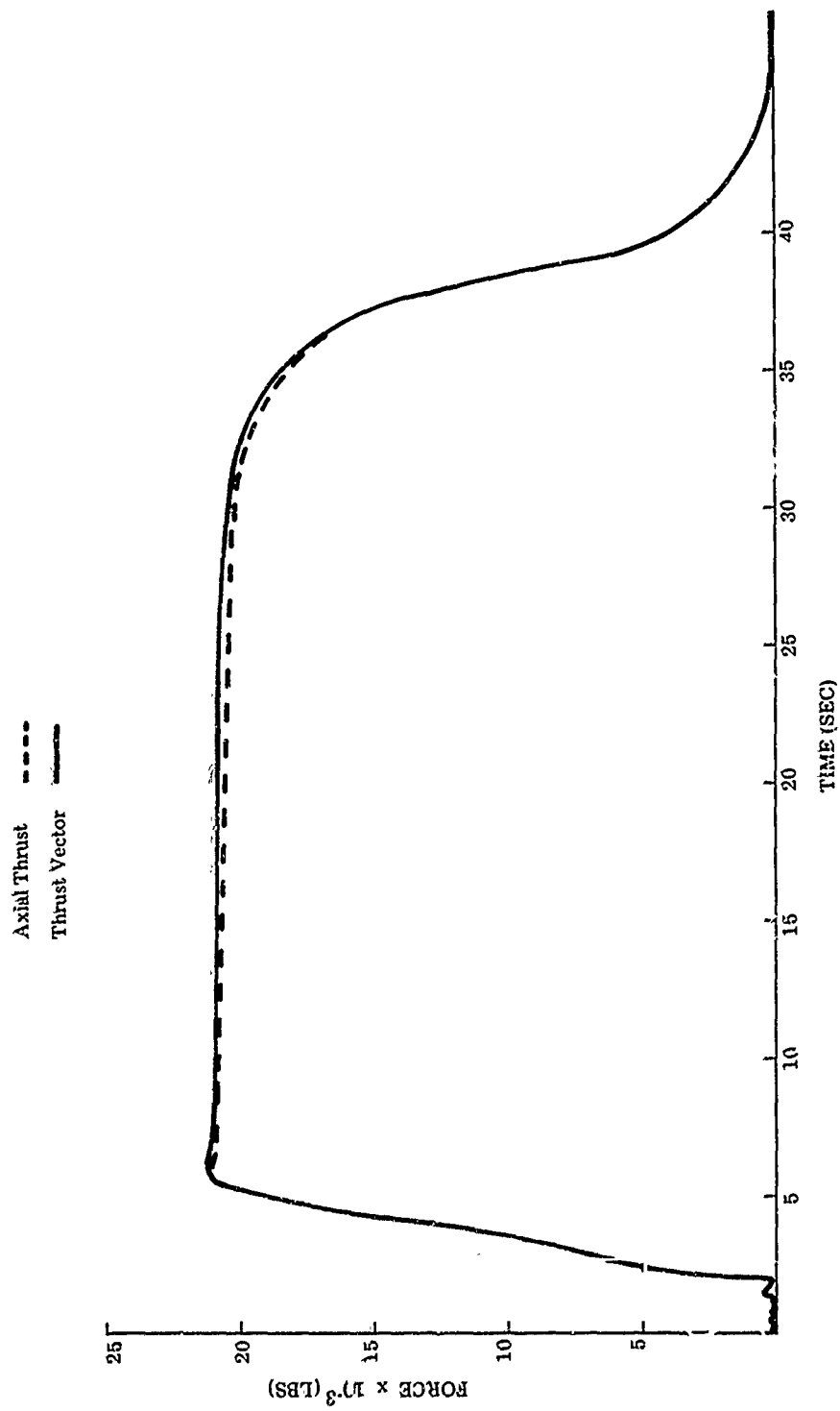


Figure 23. Axial Thrust and Thrust Vector versus Time

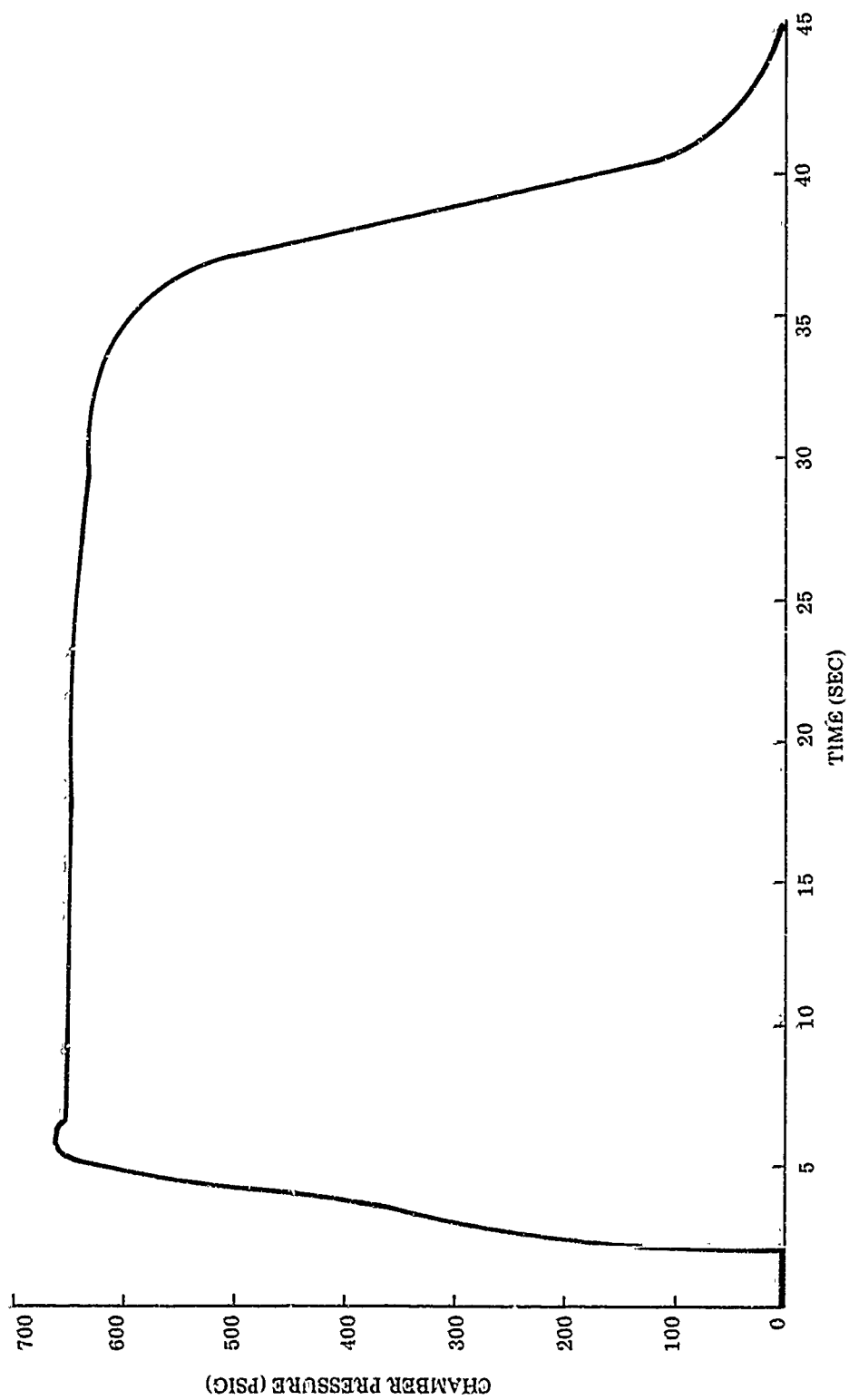


Figure 24. Chamber Pressure versus Time

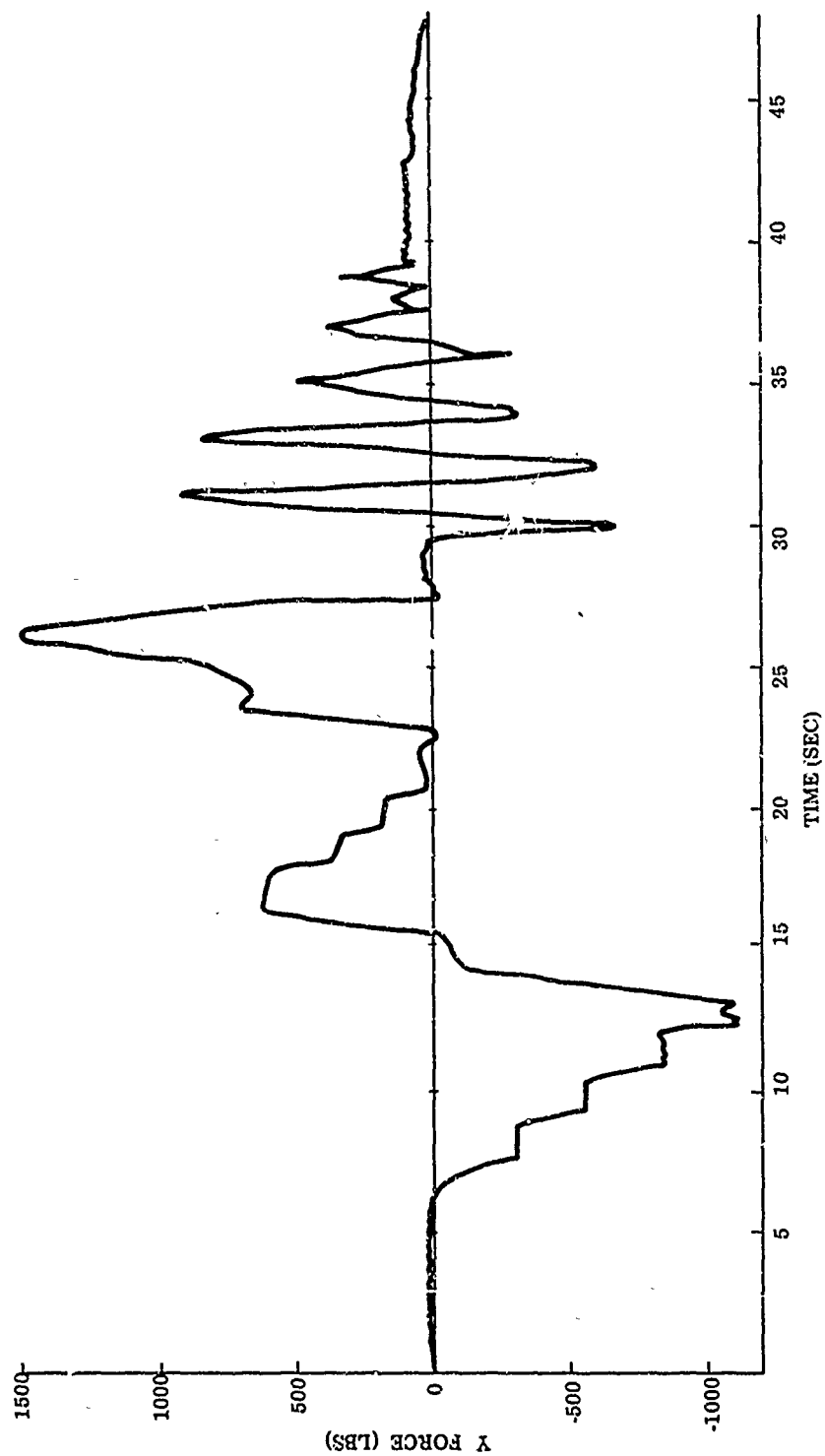


Figure 25. Y Side Force versus Time

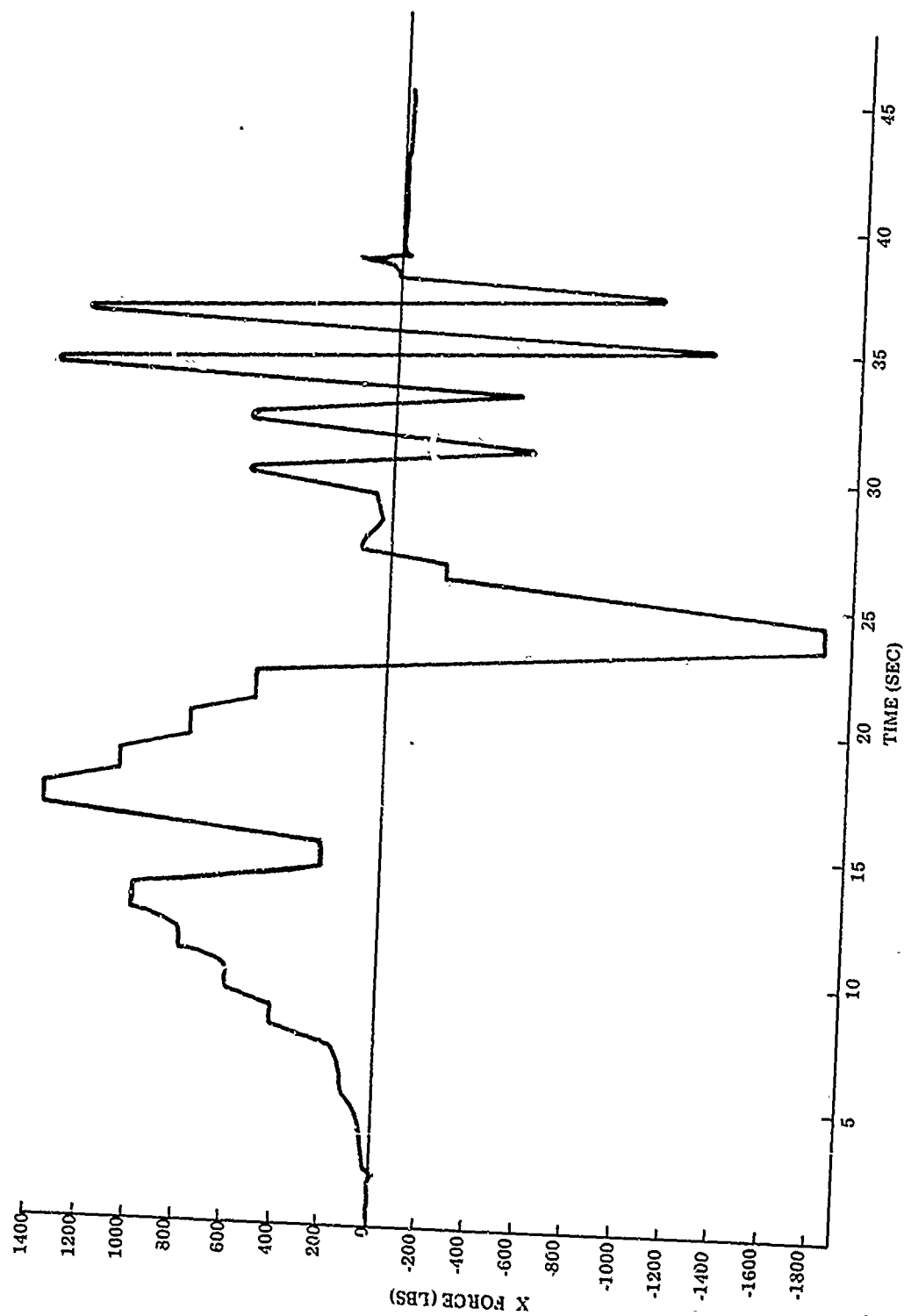


Figure 26. X Side Force versus Time

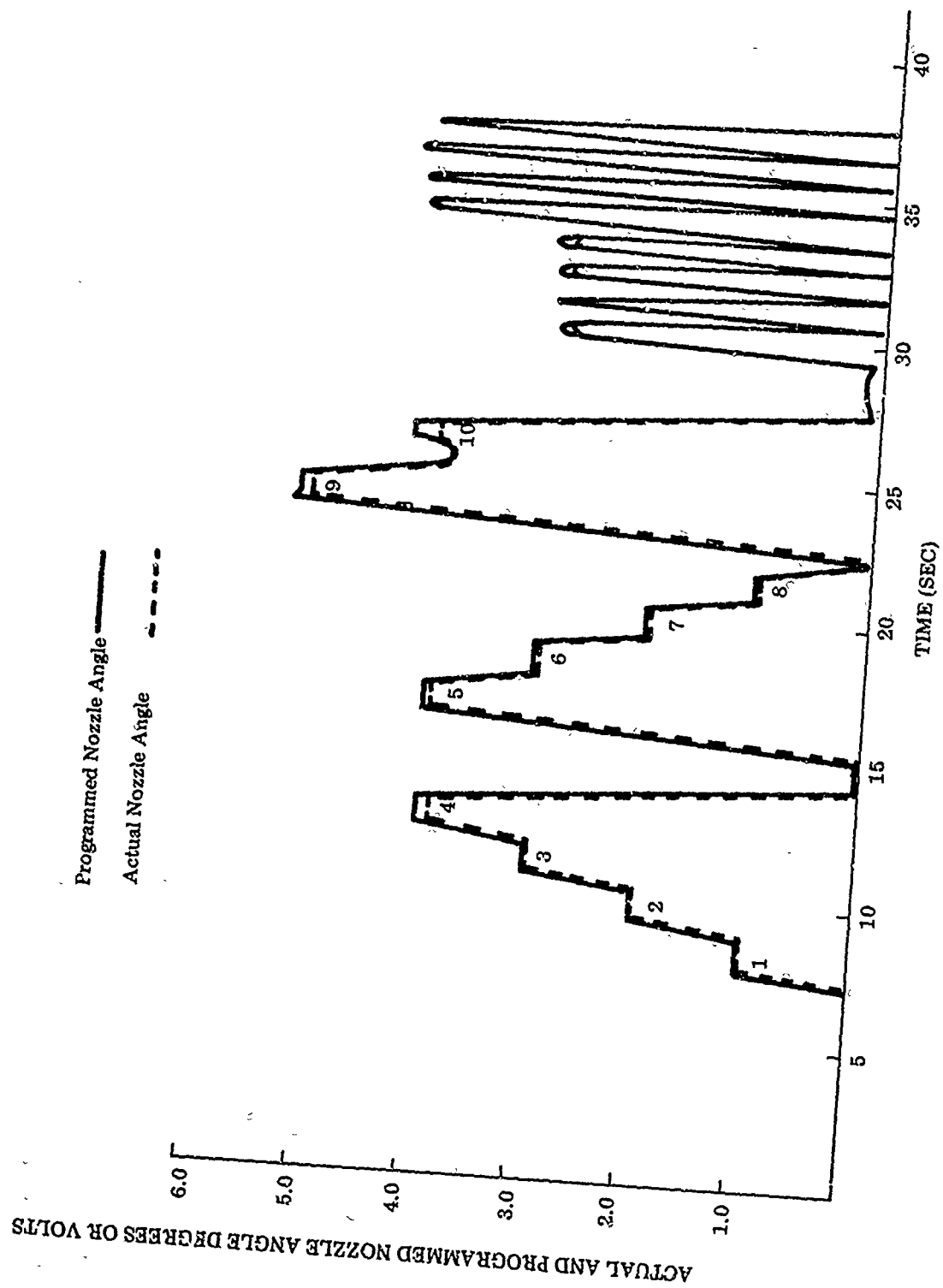


Figure 27. Actual Nozzle Angle and Programmed Nozzle Angle versus Time

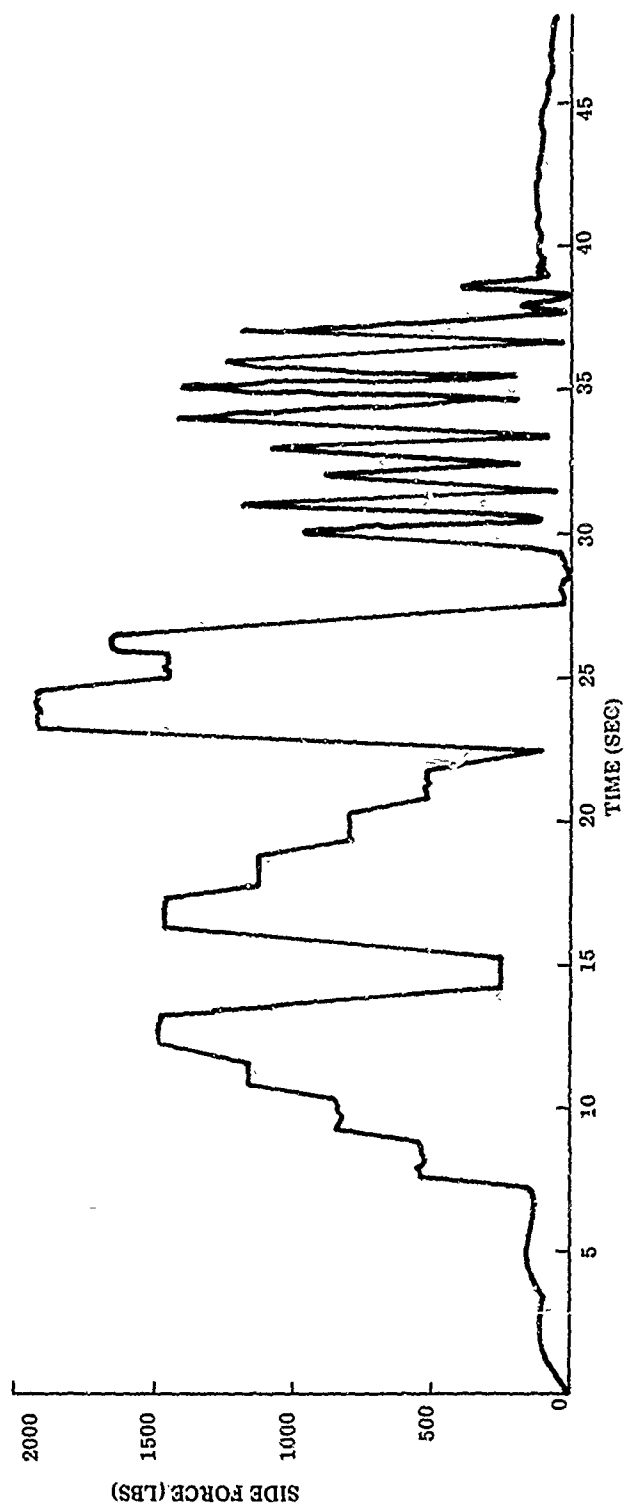


Figure 28. Side Force versus Time

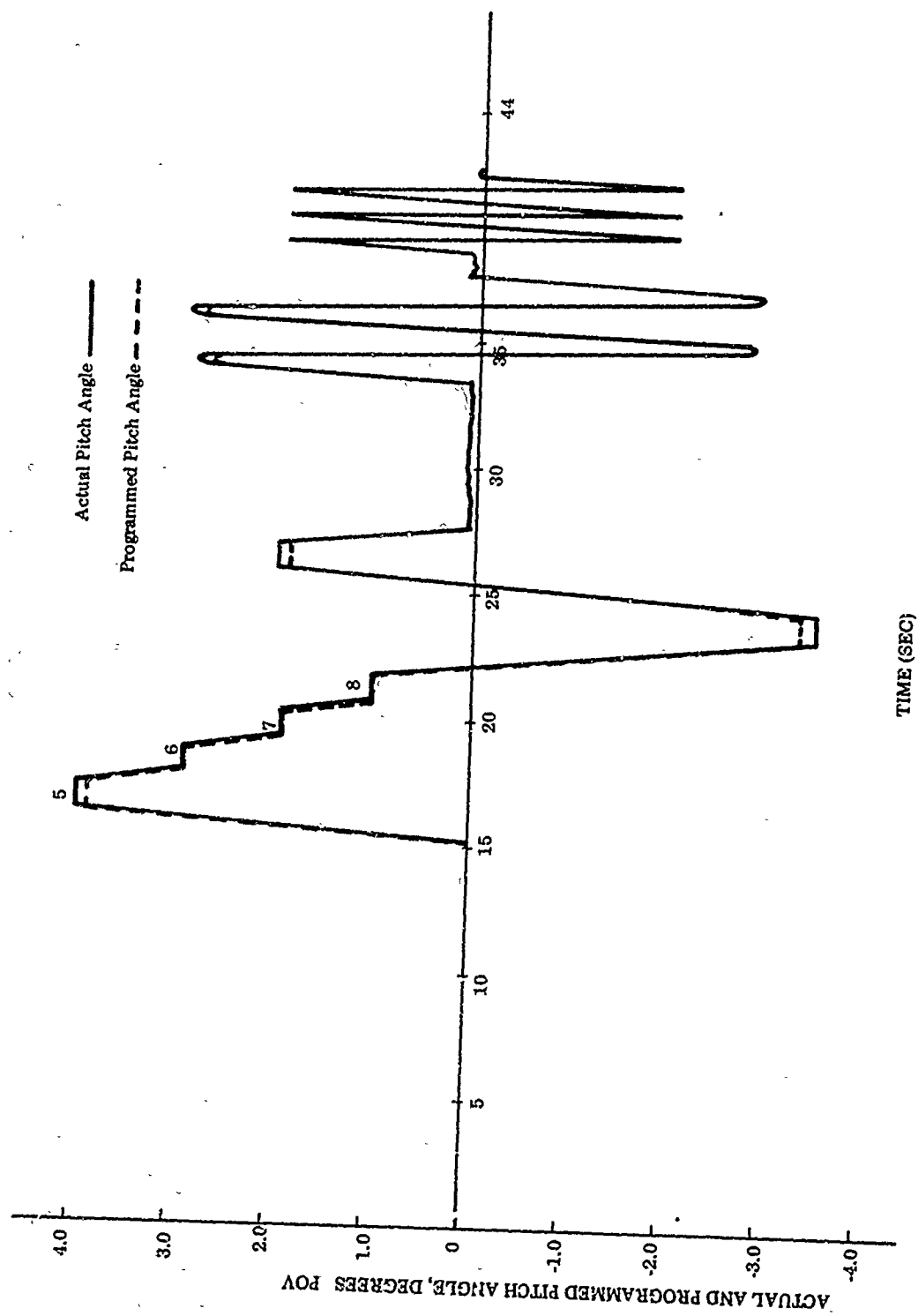


Figure 29. Actual Pitch Angle versus Time



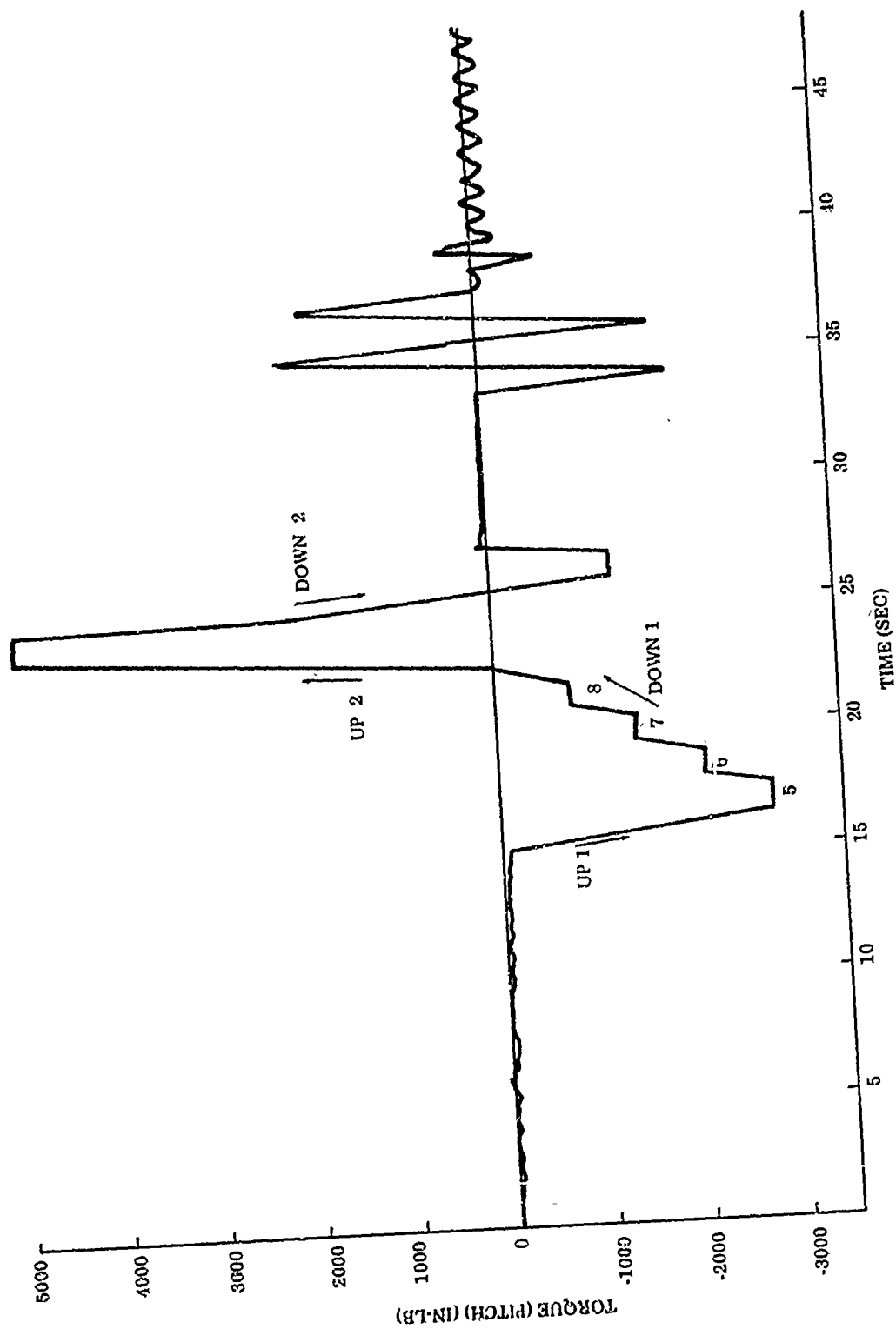


Figure 30. Torque (Pitch) versus Time

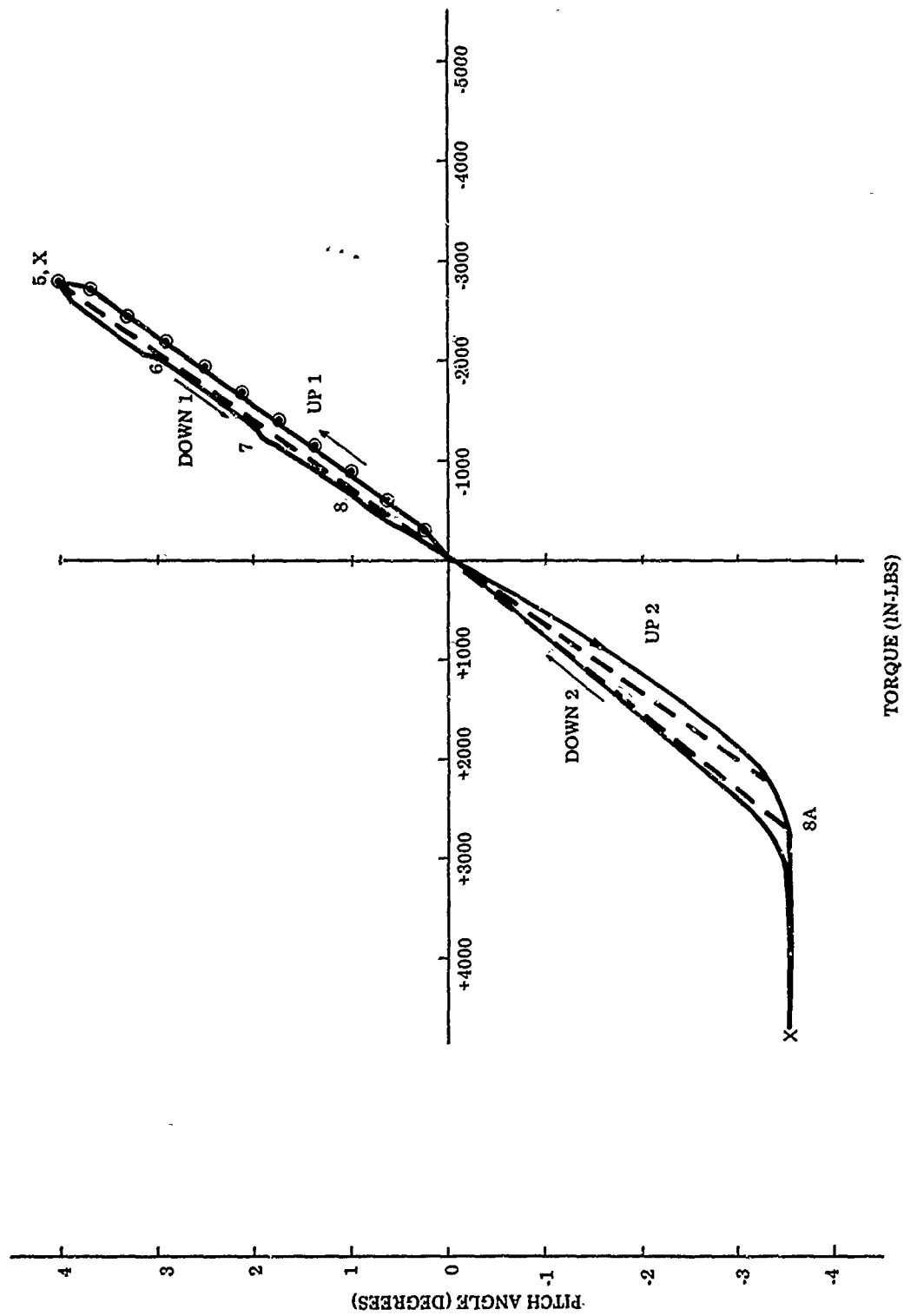


Figure 31. Pitch Angle versus Torque

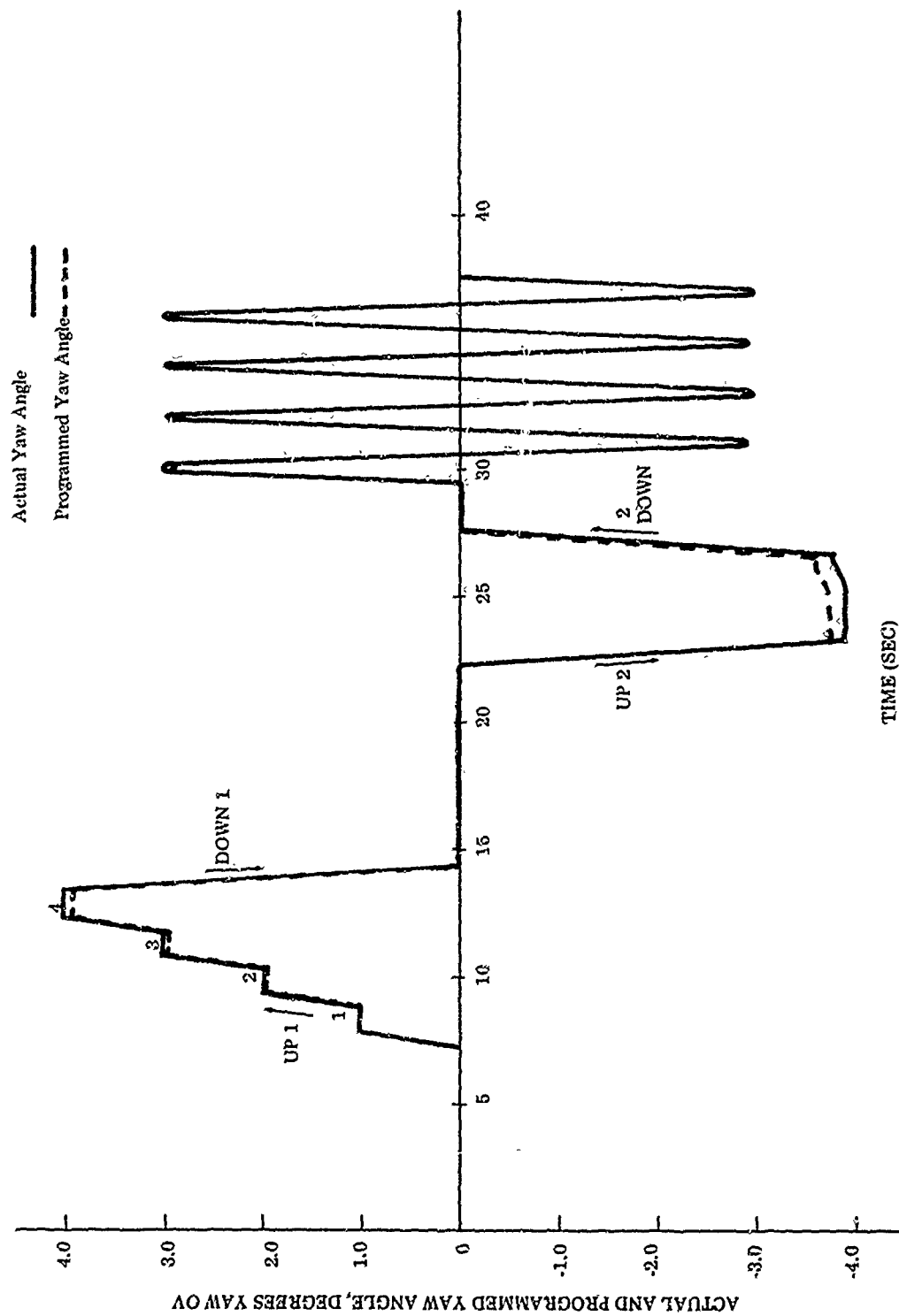


Figure 32. Actual Yaw Angle versus Time

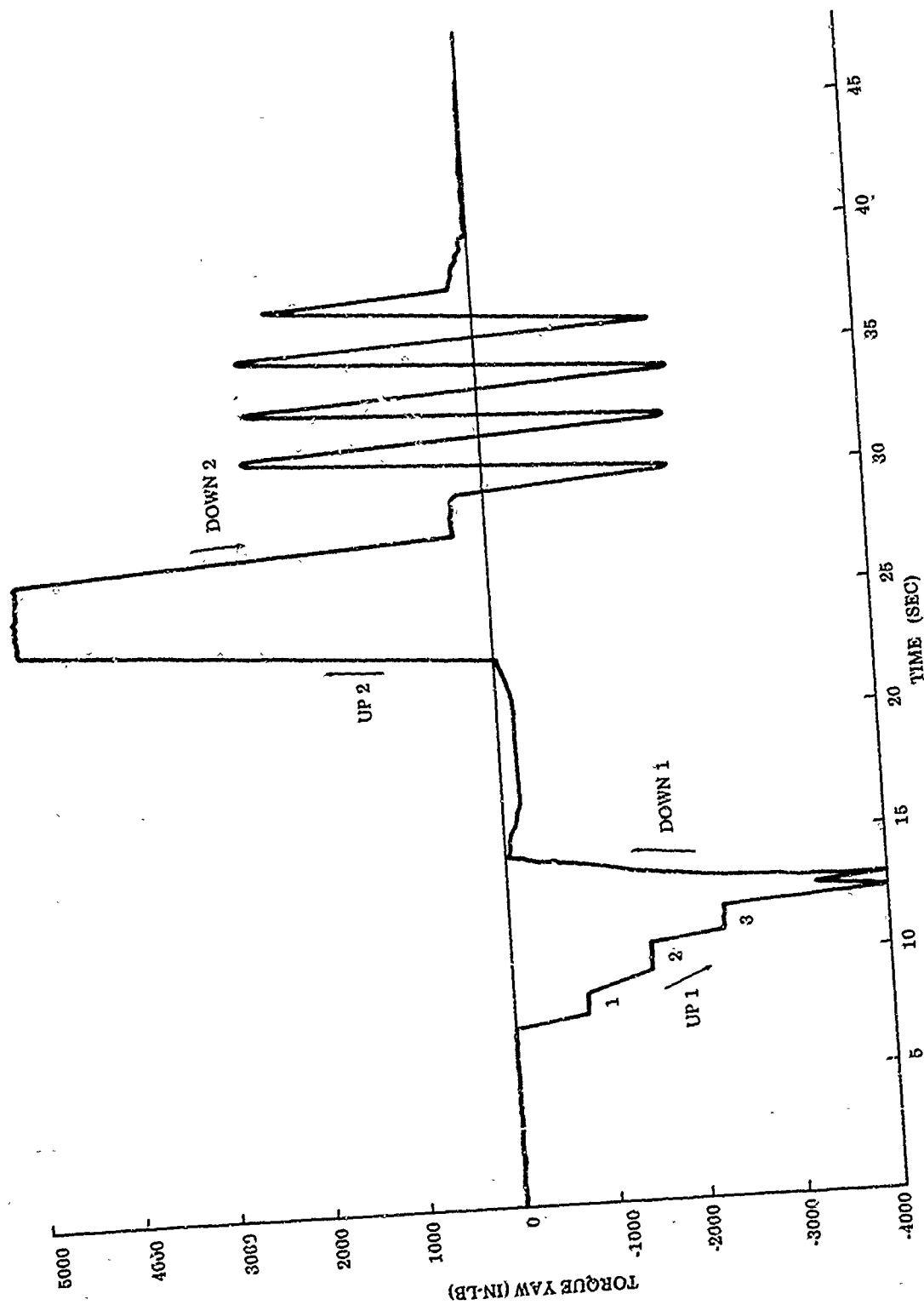


Figure 33. Torque (Yaw) versus Time

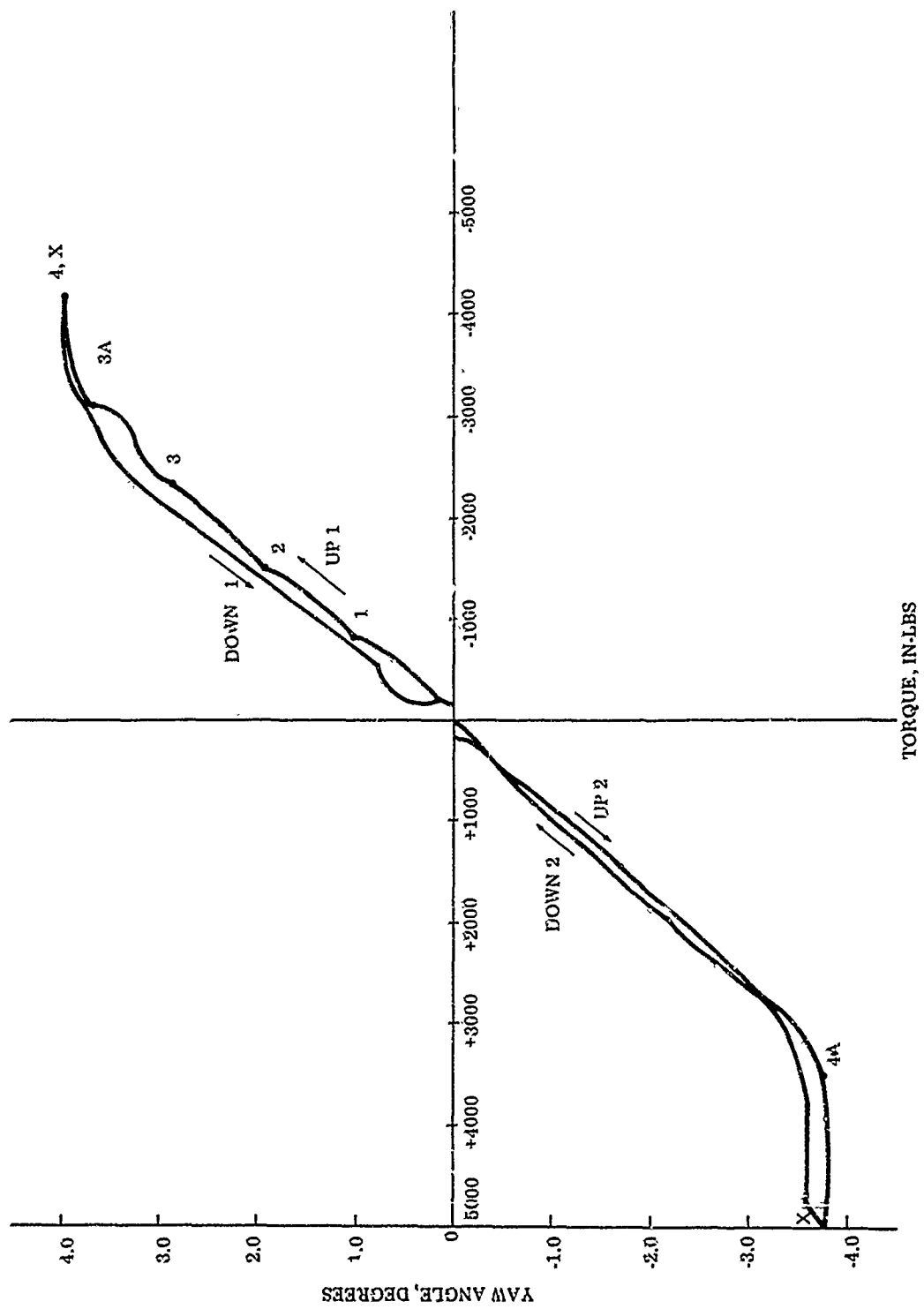


Figure 34. Yaw Angle versus Torque

NOTE: Numbers refer to positions where nozzle is not being actuated as on Figure 18, actual nozzle angle.

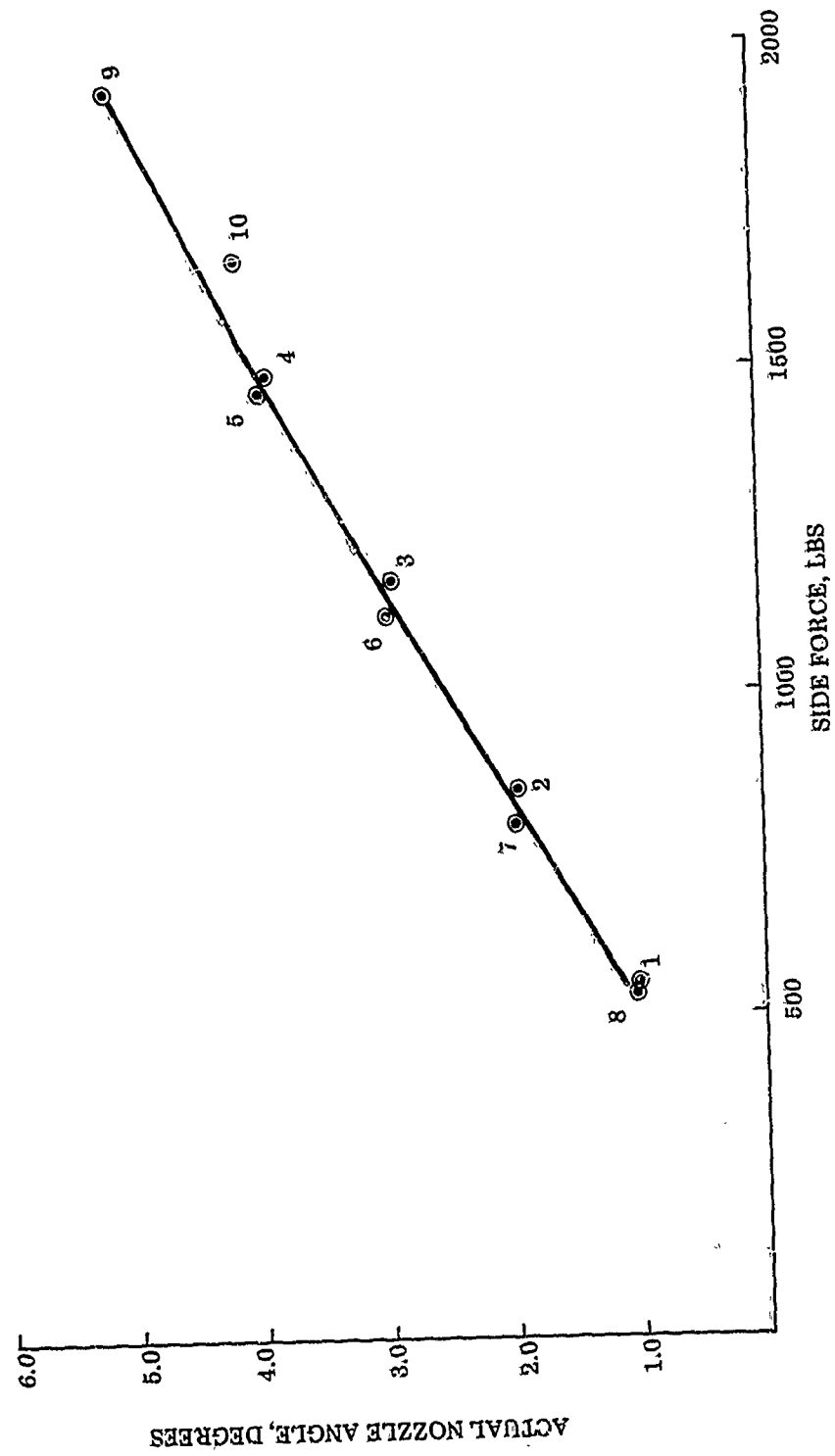


Figure 35. Actual Nozzle Angle versus Side Force

## REFERENCES

1. Strome, R.K. ; "Evaluation of a Six-component Thrust Stand,"  
AFRPL-TR-69-151.

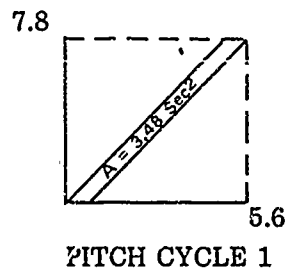
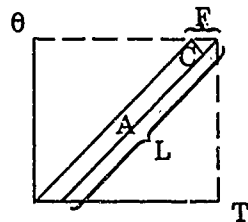
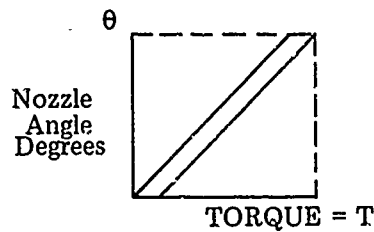
APPENDIX  
CALCULATIONS AND SYSTEM CHECKOUT



## APPENDIX

### CALCULATIONS AND SYSTEM CHECKOUT

#### A. CALCULATION OF FRICTION TORQUE



A typical torque versus angle plot is shown in the sketch. The area inside the curve is given by  $A$ , which was measured off the plots. The amount of friction torque, which is given by  $F$  in the sketch, is calculated using the following relations.

$$\sqrt{T^2 + e^2} \approx L$$

$$C \cdot L = A \Rightarrow C = \frac{A}{L}$$

$$\frac{F}{C} = \frac{L}{\theta} = F = \frac{CL}{\theta}$$

where  $C$  and  $L$  are used to describe the geometry and have no physical significance, and  $A$  is the area inside the plots.

$T$ ,  $\theta$  and  $A$  are given, thus  $F$  can be found from the above relations.  $T$ ,  $\theta$  and  $A$  will be left in the units of sections and after the calculation, the units of sections will be transformed to units of torque by the relationship that  $\text{unit}^2 = 500$  in-lb of torque

$$T = 2800 \text{ in-lb} = 5.6 \text{ units}$$

$$\theta = 3.9 \text{ degrees} = 7.8 \text{ units}$$

$$A = 3.48 \text{ units}^2$$

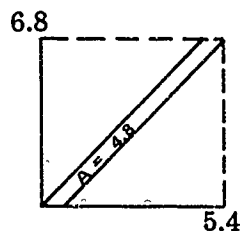
$$L = \sqrt{5.6^2 + 7.8^2} = 9.6 \text{ units}$$

$$C = \frac{3.48}{9.6} = .3625 \text{ units}$$

$$F = .3625 \frac{9.6}{7.8} = .446 \text{ units}$$

$$F = .446 \text{ units} \times 500 \frac{\text{in-lb}}{\text{unit}} = 223 \text{ in-lb}$$

#### PITCH CYCLE 2



$$T = 2700 \text{ in-lb} = 5.4 \text{ units}$$

$$\theta = 3.4 \text{ degrees} = 6.8 \text{ units}$$

$$A = 4.8 \text{ units}^2$$

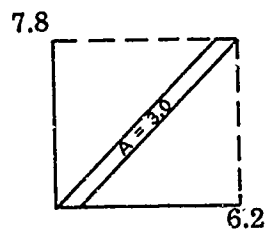
$$L = \sqrt{5.4^2 + 6.8^2} = 8.68 \text{ units}$$

$$C = \frac{4.8}{8.68} = .553 \text{ units}$$

$$F = .553 \frac{8.68}{6.8} = .706 \text{ units}$$

$$F = .706 \times 500 = 353 \text{ in-lb}$$

#### YAW CYCLE 1



$$T = 3100 \text{ in-lb} = 6.2 \text{ units}$$

$$\theta = 3.9 \text{ degrees} = 7.8 \text{ units}$$

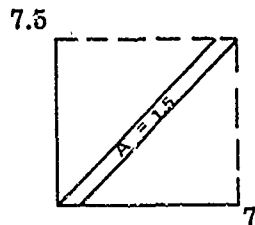
$$A = 3.0 \text{ units}^2$$

$$L = \sqrt{6.2^2 + 7.8^2} = 9.96 \text{ units}$$

$$C = \frac{3}{9.96} = .3012 \text{ units}$$

$$F = .3012 \times \frac{9.96}{7.8} = .3846 \text{ units}$$

# YAW CYCLE 2



$$F = .3846 \times 500 = 192 \text{ in-lb}$$

$$T = 3500 \text{ in-lb} = 7 \text{ units}$$

$$\theta = 3.75 \text{ degrees} = 7.5 \text{ units}$$

$$A = 1.5 \text{ units}^2$$

$$L = \sqrt{7^2 + 7.5^2} = 10.26 \text{ units}$$

$$C = \frac{1.5}{10.26} = .146 \text{ units}$$

$$F = \frac{10.26}{7.5} \times .146 = .199 \text{ units}$$

$$F = .199 \times 500 = 100 \text{ in-lb}$$

## B. DETERMINATION OF TORQUE EQUATION

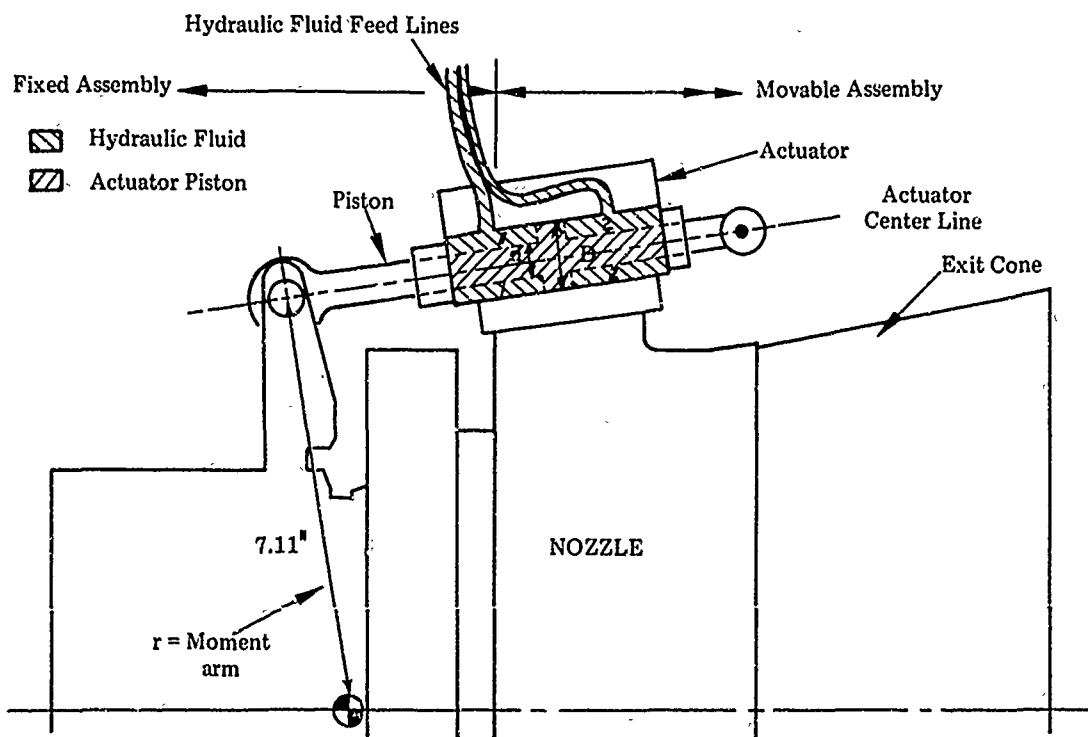


Figure 36. Nozzle Actuators

The actuator was attached to the movable assembly of the motor and reacted against the fixed assembly. Hydraulic fluid entered the actuator and created a pressure differential between stations 1 and 2. This pressure differential caused the piston to move the movable assembly. The effective area of the piston  $\left(\frac{D^2 - d^2}{4}\right)$  was equal to  $0.729 \text{ in}^2$ . The moment arm was measured to be 7.11 inches. The torque required to actuate the nozzle was then:

$$\begin{aligned} T &= r \times F & r &= 7.11 \text{ inches} \\ T &= 7.11 \text{ in} \times .729 \text{ in}^2 \times P \text{ lb} & F &= A \\ T &= 5.183 P \text{ in-lb} & &= AP (.729 \text{ in}^2) \end{aligned}$$

P in terms of Yaw is (Yaw P - Yaw R)

P in terms of Pitch is (PP-PR)

### C. NOZZLE BALLISTIC PERFORMANCE

$$\begin{aligned} \text{Nozzle Efficiency (N}_c\text{) Percent} &= \frac{C_f (\text{calculated})}{C_f (\text{theoretical})} \times 100 \\ &= \frac{C_{fd}}{C_{fi}} \times 100 \end{aligned}$$

where  $C_{fi}$  (theoretical) is 1.864 for Type I-B propellant, for a 25:1 expansion ratio nozzle; and  $C_{fd}$  (calculated) is defined as

$$C_{fd} = C_{fi} - (\Delta C_f)_{S.L} + (\Delta C_f)_{-M} + (\Delta C_f)_{P.G} = C_{fi} - \Delta C_{f_{net}}$$

where

$(\Delta C_f)_{-M}$  = Performance loss due to gas phase Mach number asymmetry and flow angularity effects in null position.

$(\Delta C_f)_{S,L}$  = Performance loss due to nozzle split-line in null position.

$(\Delta C_f)_{P-G}$  = Performance loss due to transonic throat region particle gas velocity lag losses.

The above shows the equations used for the calculation of  $N_c$ . No data for the individual terms were available.

#### D. TVC SYSTEM CHECKOUT

The purpose of the TVC system checkout was to verify the system operation and data acquisition system integrity. The nozzle was operated through the entire duty cycle in two different manners to determine if the TVC system and nozzle were operating properly. First, the nozzle was tested with the use of a pressure test stand with gaseous nitrogen under a pressure of 83 psig (83 psig was the approximate pressure that was predicted for the O-ring seal during the firing). This checkout was to test for gas leakage around the seal where the movable and nonmovable portions of the nozzle interfaced and to test for proper operation of the seal. Second, the TVC system was operated in the unpressurized mode.

The controller (programmer) system for the TVC system was the main source of problems during the checkout. The controller (FM tape) system motor drive was slow in building up speed after the "on" command was given. As the tape drive accelerated, the FM reproduce unit first saturated and produced a full capacity signal which appeared as a spike in the duty cycle command voltage, and after a short period of time the signal decayed to the zero level of the recorded signal. An open circuit, the zero level of the recorded signal, occurred just as the tape motor drive reached the correct operating speed. The input to the nozzle TVC system must be

a within range dc command signal or a shorted input, and never an open circuit. A voltage spike or an open circuit, occurring during the tape acceleration time, would cause the nozzle actuators to extend to their limits and the nozzle to go hard over and hit the stops causing physical damage and possible zero shifts. In an attempt to reduce the possibility of a voltage spike or open circuit, a 1-second time delay shorting relay was inserted in the command lines. As the tape unit TVC system command lines built up speed, the short prevented the command lines from "seeing" the open circuit or voltage spike. After 1 second, when the tape drive was at the correct operating speed, the short was no longer in effect and the normal duty cycle command voltage was input to the TVC system command lines. During normal operation, the time delay electrical short could cause the nozzle to go past the programmed 4.0 degree angle and hit the stops. To reduce the possibility of the nozzle hitting the stops, the input voltage was reduced from 4.0 volts to approximately 3.9 volts. This was equivalent to reducing the amount the nozzle could move from 4.0 to 3.9 degrees. Thus, since the short could have caused the nozzle to go past 4.0 degrees, the amount the nozzle traveled was reduced so it would not rotate past approximately 4.0 degrees.

During the preliminary actuation tests, the nozzle continually went past the programmed 4-degree angle and contacted the stops. At first, it was thought that this hard over condition was caused by both bad pitch and yaw potentiometers. These were replaced with two extra potentiometers that were supplied with the TVC equipment. Later, it was found that the voltage spike, which caused the nozzle to go hard over, was partially being caused by a bad potentiometer in the feedback channel. There were two channels, and the potentiometer in the instrumentation channel was found to be functioning properly. The instrumentation and feedback wiring were then reversed to eliminate this cause of the spike. The nozzle no longer "saw" a spike in the electrical signal that was input to the pitch and yaw potentiometers by the new feedback channel, and the spike in the new instrumentation channel could be accounted for.

A problem that was encountered during the entire checkout was zero shift as read in the digital acquisition system visual display. At first it was thought that a majority of the problem came from the pitch and yaw potentiometers used to electrically actuate the system. The digital acquisition system could record the adjusted zero of the potentiometer to about  $0 \pm 20$  counts out of 8000 counts; this was used as the initial zero. After the nozzle was actuated and set back to zero mechanically, the electrical zero would shift about 1000 counts. This was partially caused by slippage in the jack shaft rod which was attached to the wiper arms in the potentiometer. The potentiometer was opened and the jack shaft rod tightened. This operation was not successful because there was still slippage in the mechanism. The rod was then welded to the wiper arms, which seemed to work satisfactorily until it was found that the heat from the weld might have damaged the internal components of the potentiometer. The potentiometers that were originally used replaced the damaged items. This left the actuation system in its original configuration. Another possible source of the zero shift problem was attributed to the FM tape system that was used to feed the duty cycle to the nozzle actuation system. The FM tape system was originally designed to record data during a firing. This tape was the digital tape that was sent to the computer for data reduction. Since there was no other tape system available, the FM tape was used to input the duty cycle into the actuation system. The characteristics of the FM tape could have caused some zero shift. This problem was not remedied before the firing because there was no other system available to do the job. The zero shift partially caused the spike in the data acquisition system. 8000 counts on the digital system was equivalent to the maximum 4 degrees of nozzle movement. Thus, if there was a zero shift of 600 counts during the actuation, the digital acquisition system would record that the nozzle would move to -7400 and +8600 counts by the end of the test. Since about 8300 counts was the farthest the nozzle could move electrically, it would contact the stops when it got to that value. As mentioned earlier, the input voltage was reduced sufficiently to prevent the nozzle from going over hard and hitting the stops.

## E. PLOTS



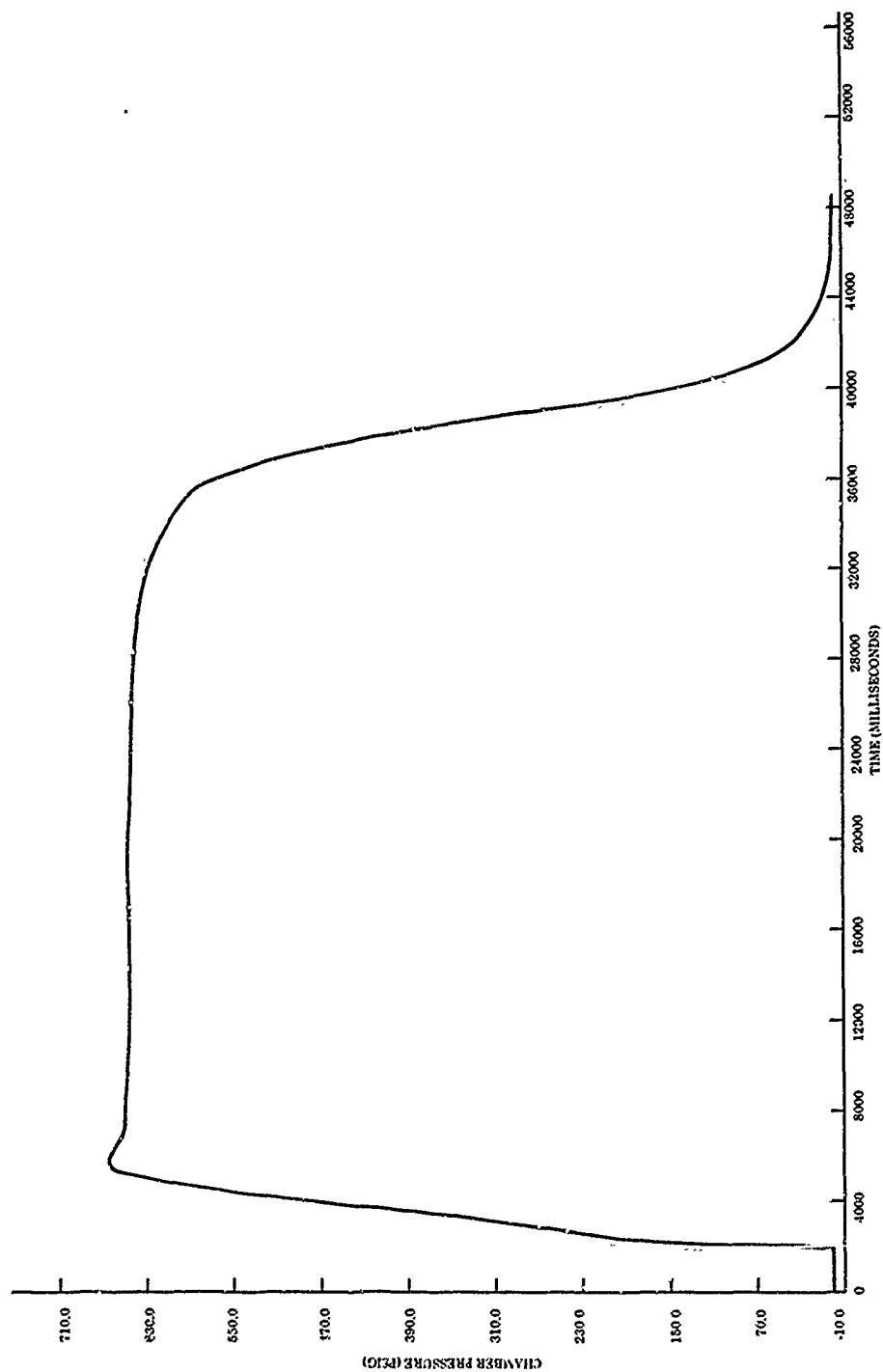


Figure 37. Plotted Chamber Pressure

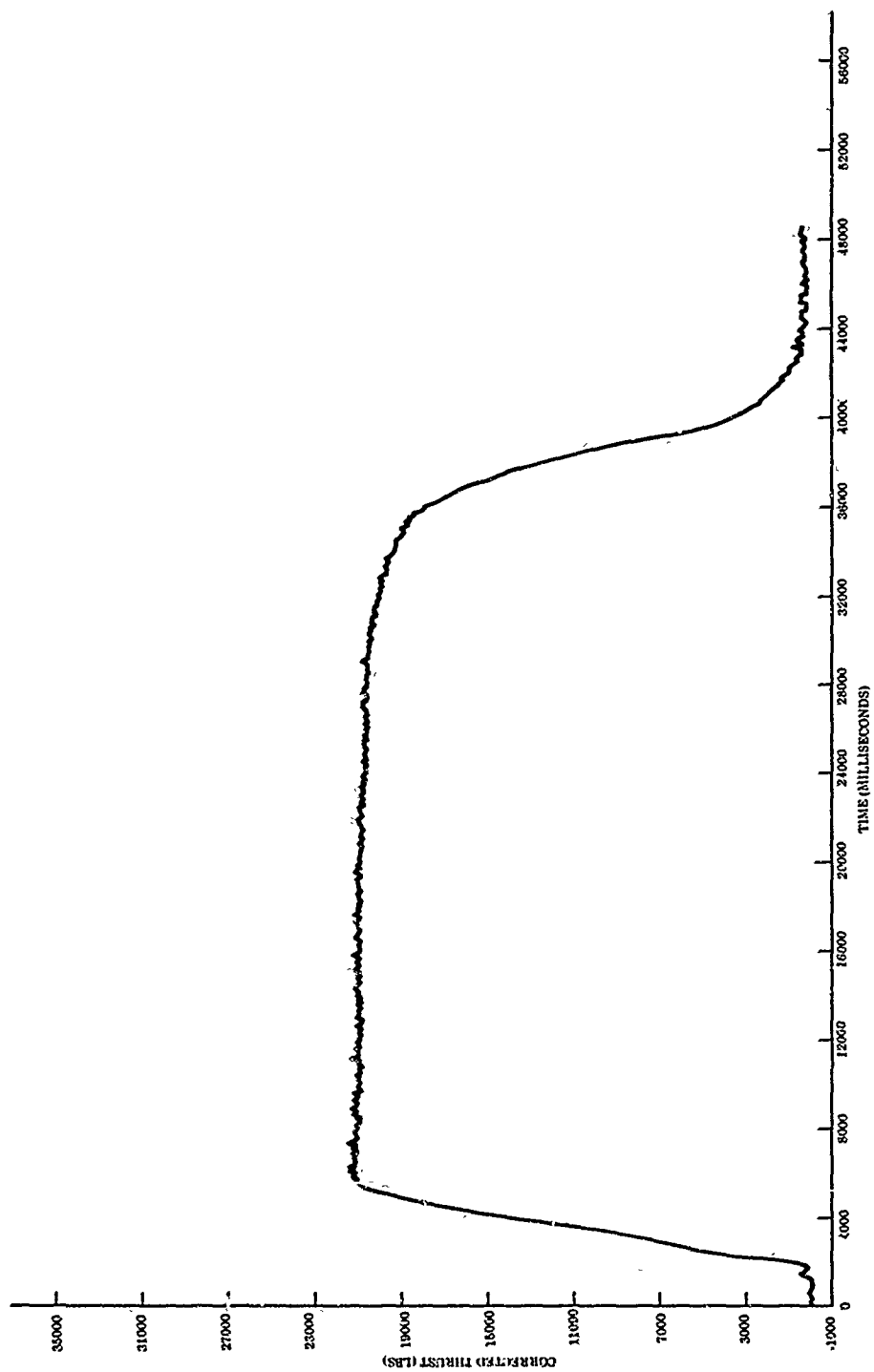


Figure 38. Plotted Thrust

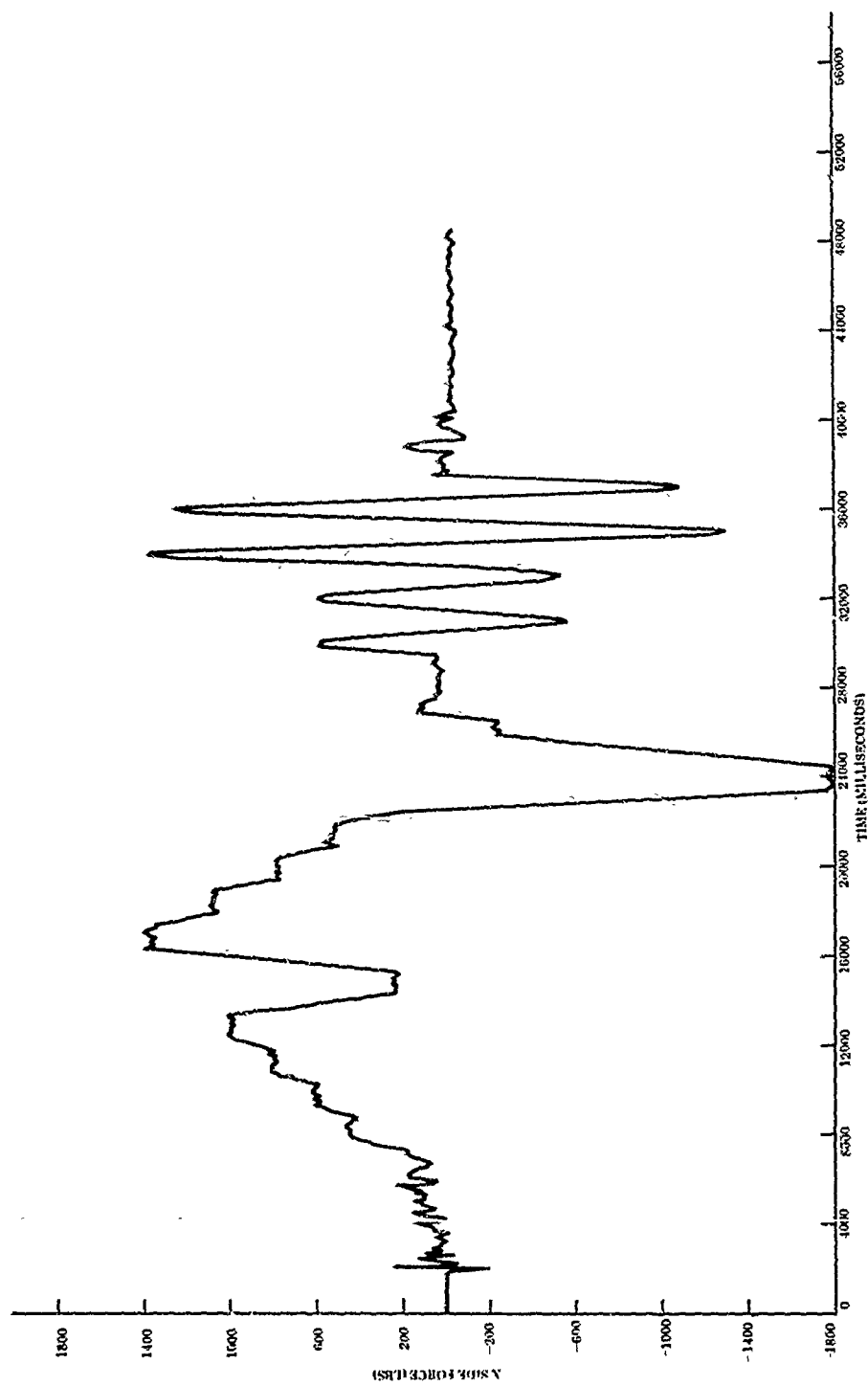


Figure 39. Plotted X Side Force

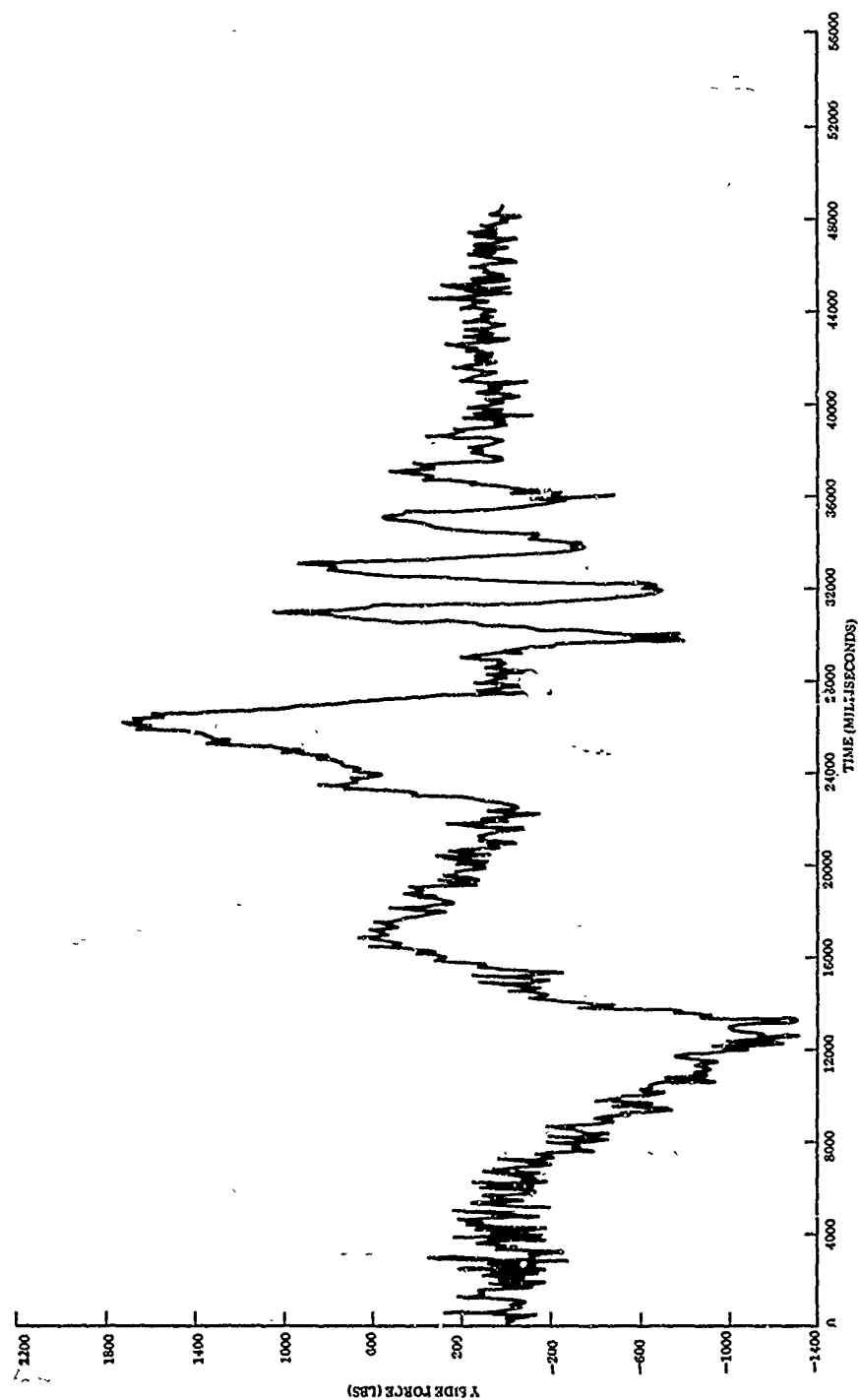


Figure 40. Y Side Force

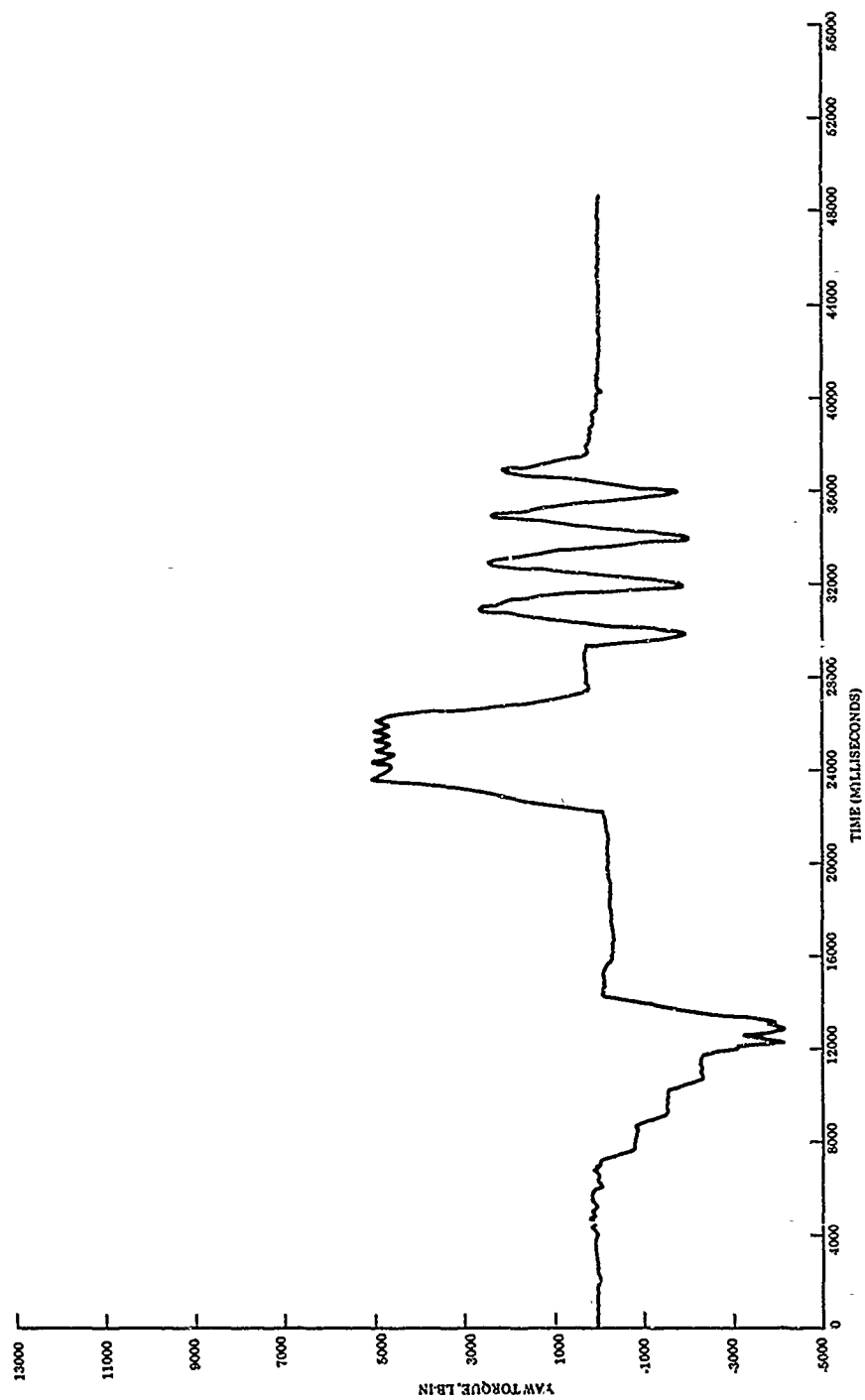


Figure 41. Yaw Torque

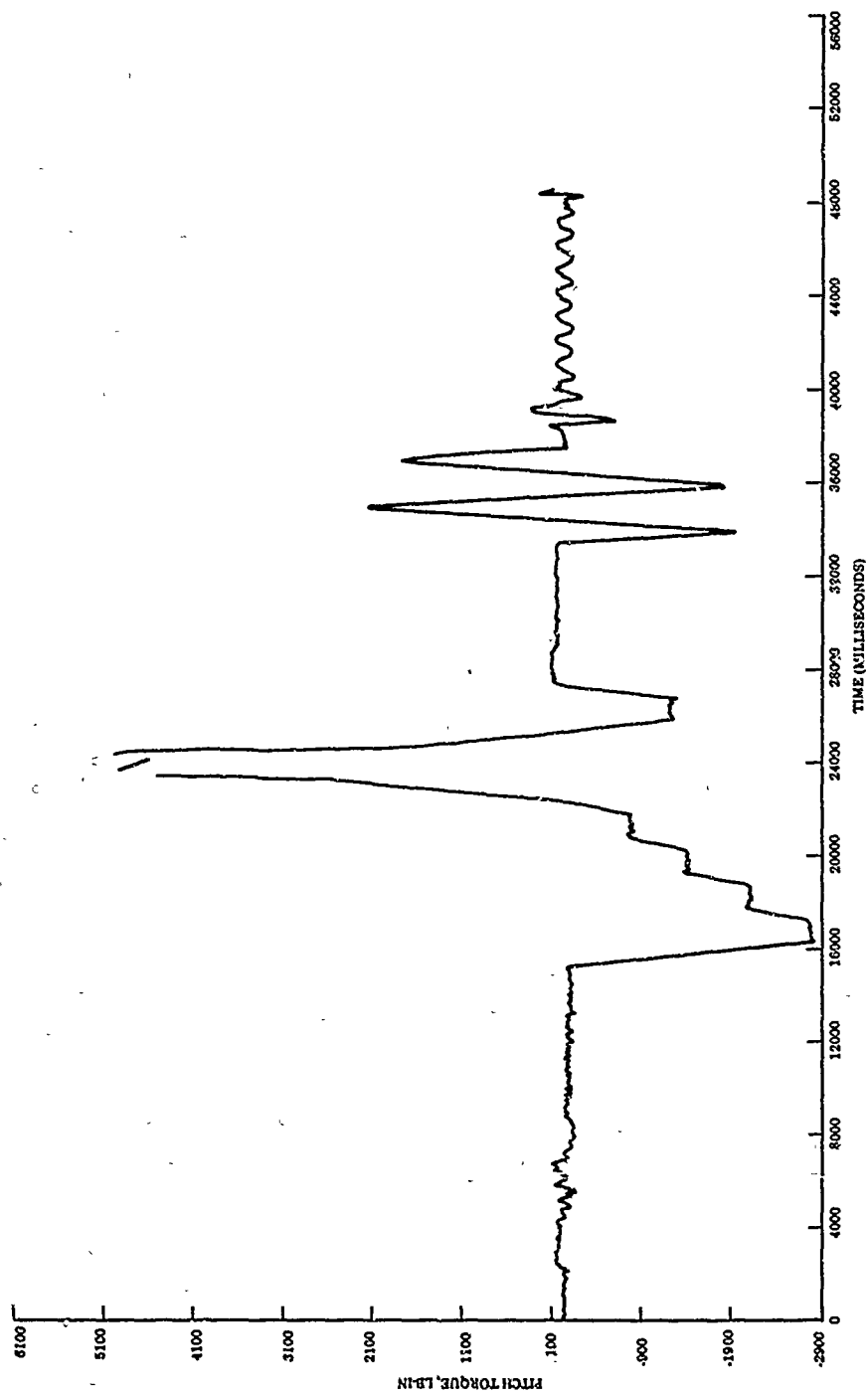


Figure 42. Plotted Pitch Torque

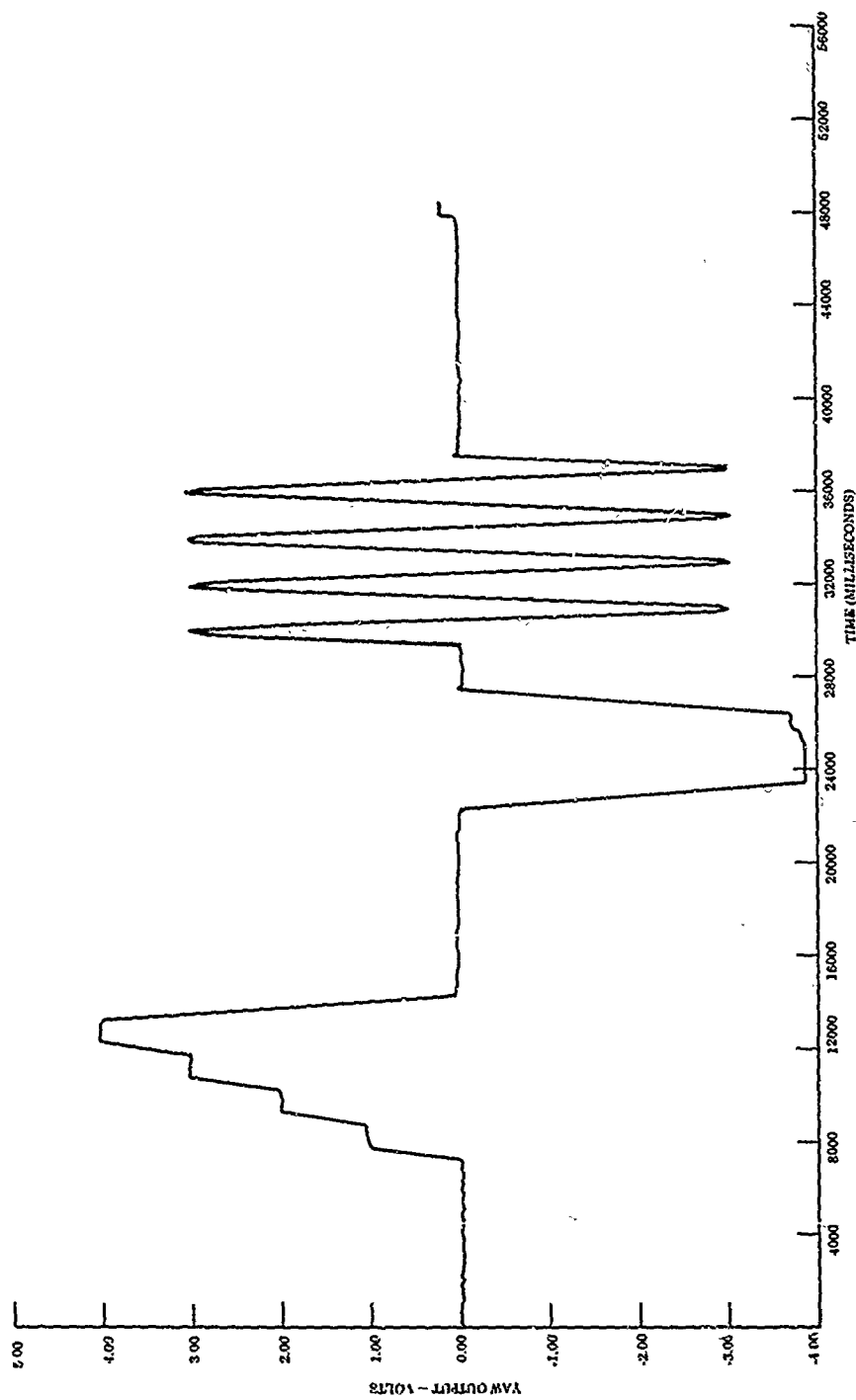


Figure 43. Yaw Output Volts

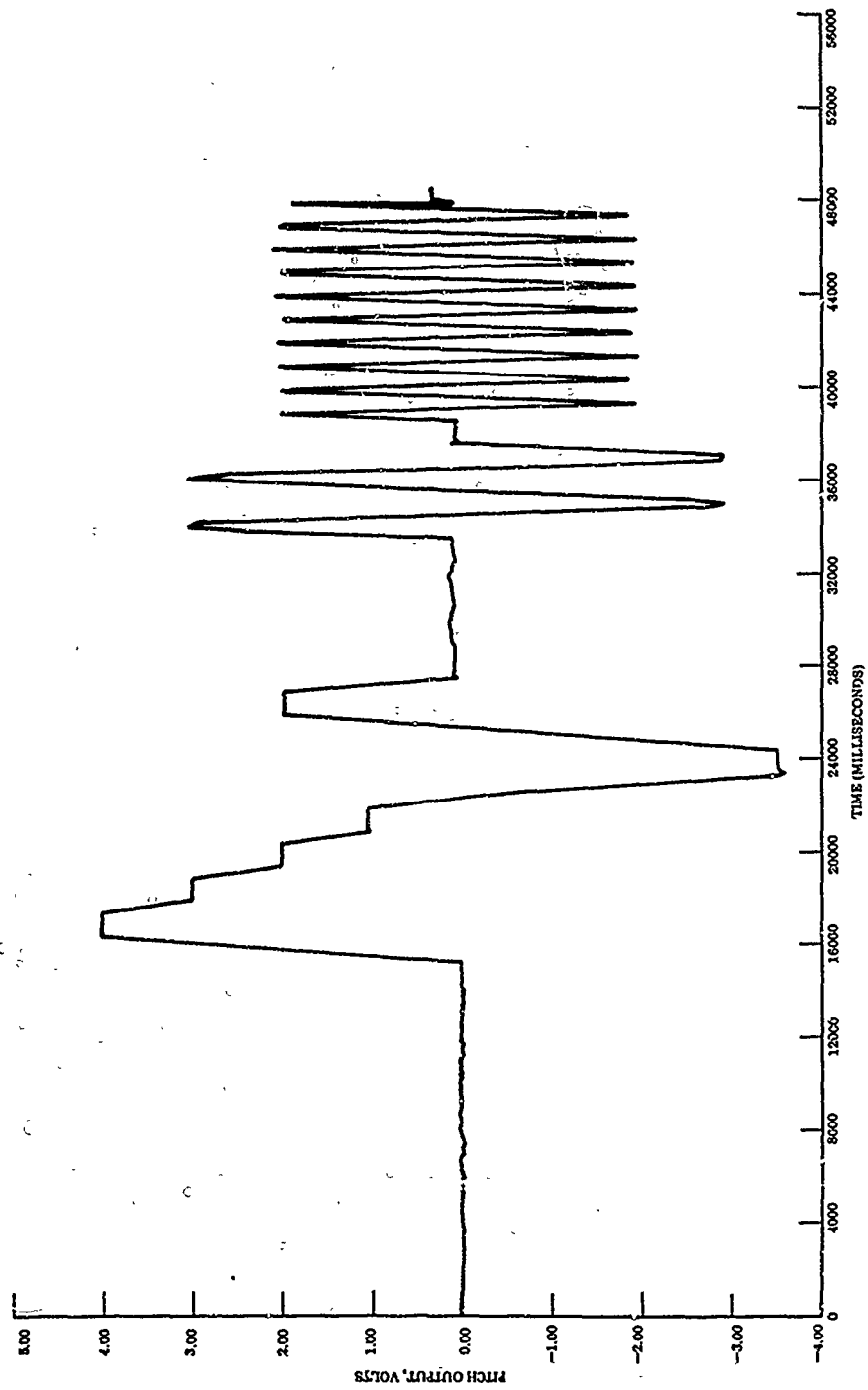


Figure 44. Pitch Output Volts



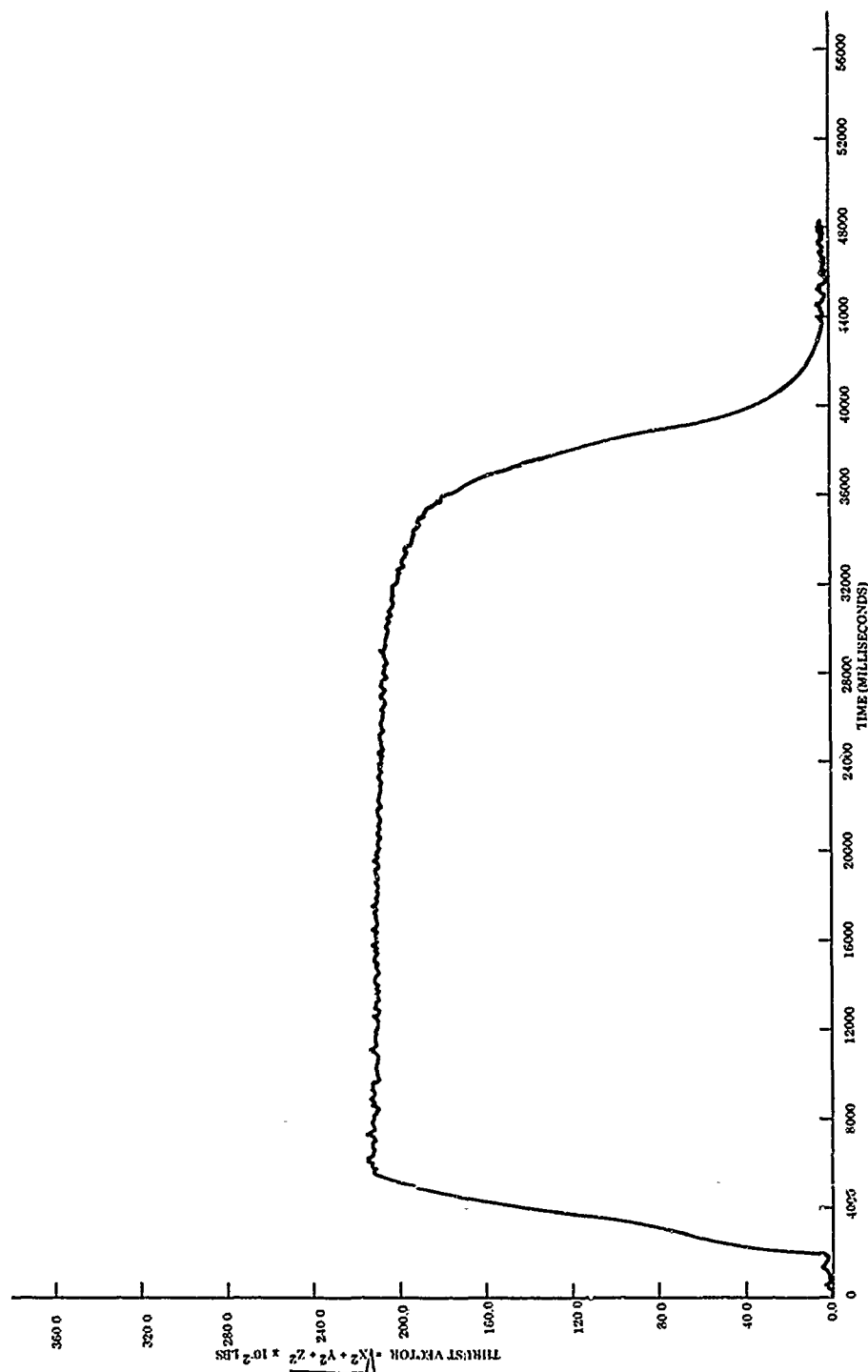


Figure 45. Plotted Thrust Vector

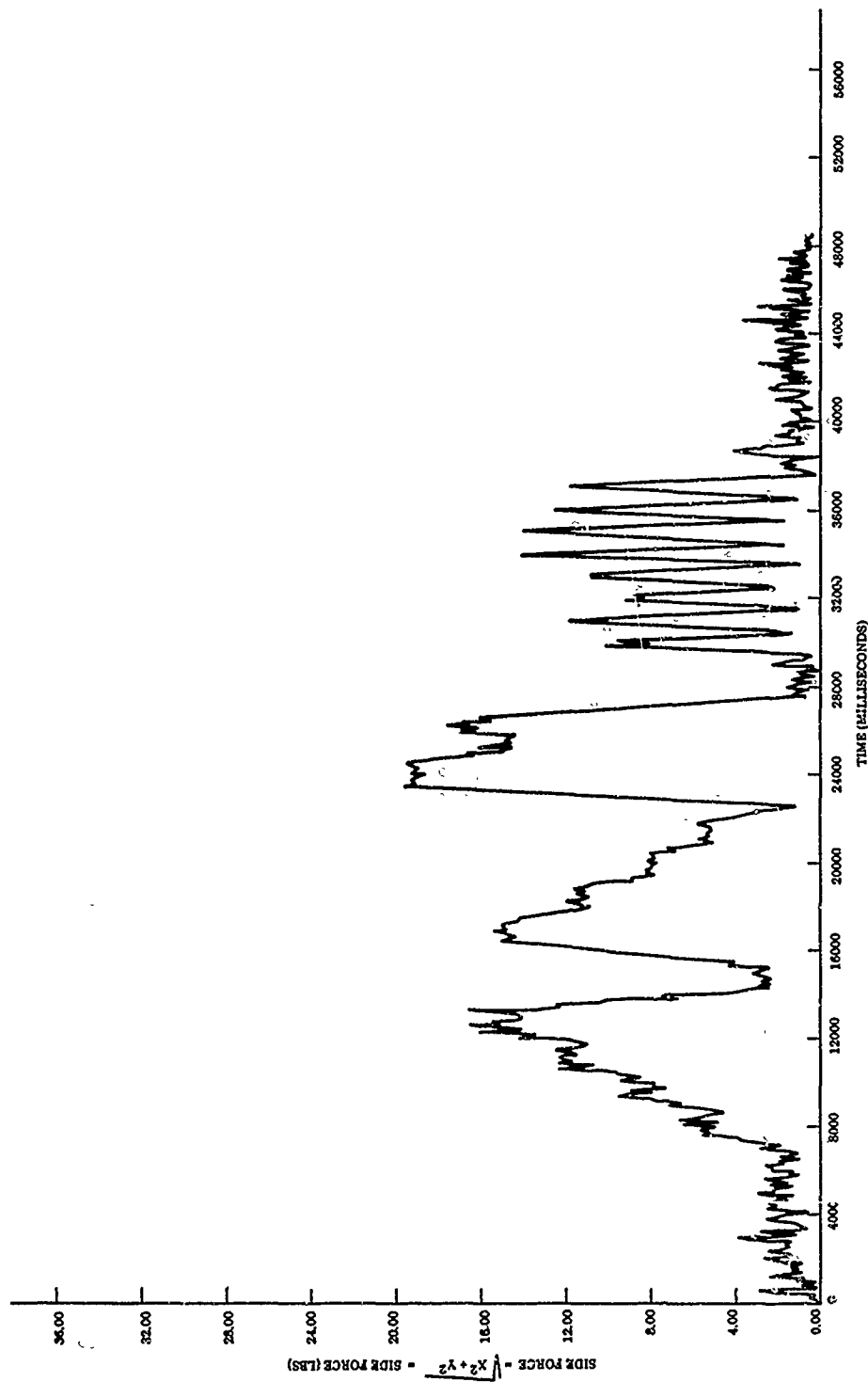


Figure 46. Plotted Side Force

Unclassified

Security Classification

DOCUMENT CONTROL DATA - R & D		
(Security classification of title, body of abstract and indexing annotation must be entered when the overall report is classified)		
1. ORIGINATING ACTIVITY (Corporate author) Air Force Rocket Propulsion Laboratory Edwards, California 93523		2a. REPORT SECURITY CLASSIFICATION Unclassified
		2b. GROUP N/A
3. REPORT TITLE Test Firing of a Supersonic Split-Line Nozzle		
4. DESCRIPTIVE NOTES (Type of report and inclusive dates) Test Report, 29 January 1969		
5. AUTHOR(S) (First name, middle initial, last name) Richard K. Strome, Lt, USAF		
6. REPORT DATE October 1969	7a. TOTAL NO. OF PAGES 94	7b. NO. OF REFS 1
8a. CONTRACT OR GRANT NO.  b. PROJECT NO. 305903AMG  c.  d.		9a. ORIGINATOR'S REPORT NUMBER(S) AFRPL-TR-69-203  9b. OTHER REPORT NUMBER(S) (Any other numbers that may be assigned this report)
10. DISTRIBUTION STATEMENT This document is subject to special export controls and each transmittal to foreign governments or foreign nationals may be made only with approval of AFRPL (RPOR-STINFO), Edwards, California 93523.		
11. SUPPLEMENTARY NOTES		12. SPONSORING MILITARY ACTIVITY Air Force Rocket Propulsion Laboratory Air Force Systems Command, USAF Edwards, California 93523
13. ABSTRACT A supersonic split-line (SSSL) nozzle test was conducted on the Air Force Rocket Propulsion Laboratory (AFRPL) 84-inch Char motor, utilizing a Gilmore six-component thrust stand. The side force amplification factor was determined to be about 1.07, with an estimated maximum error of <del>±</del> 5 percent. The torque required to actuate the nozzle was determined to be about 67 in-lb per degree with a maximum vector angle of 5.2 degrees. The maximum thrust was 21,200 pounds and the nozzle produced a maximum side force of about 1920 pounds at a deflection of 5.1 degrees. Burning and average chamber pressure were 36 seconds and 640 psi, respectively. The thrust stand exhibited much dynamic ringing in one of the axes, with very little in the other. The side-force-versus-time curves were essentially parallel to the nozzle duty-cycle curves. The test was a complete success, demonstrating the supersonic split-line concept by the measurement of a side force amplification factor greater than 1.0.		

DD FORM 1 NOV 65 1473

93

Unclassified  
Security Classification

plus or minus

~~Unclassified~~  
Security Classification

14	KEY WORDS	LINK A		LINK B		LINK C	
		ROLE	WT	ROLE	WT	ROLE	WT
	Thrust Vector Control Supersonic Split-line Nozzle Thrust Stand Actuation Systems						